



# Terrestrial ion circulation in space

Masatoshi Yamauchi

Swedish Institute of Space Physics, Box 812, S-98128 Kiruna, Sweden

**Correspondence:** M. Yamauchi (M.Yamauchi@irf.se)

**Abstract.** Observations of the terrestrial ion transport and budget in the magnetosphere are reviewed, with stress on low energy ions in the high-altitude polar region and inner magnetosphere, for which Cluster significantly improved the knowledge. Outflowing ions from the ionosphere are classified into three types in terms of energy: (1) as cold ions refilling the plasmasphere faster than Jeans escape, (2) as cold supersonic ions such as the polar wind, and (3) as suprathermal ions energized by wave-particle interaction or parallel potential acceleration. Majority of the suprathermal ions are further energized at higher altitudes becoming "hot" with much higher velocity than the escape velocity even for heavy ions. This makes heavy ions in this category more abundant than cold refilling or cold supersonic flow.

The immediate destination of these terrestrial ions varies from the plasmasphere, the inner magnetosphere including those entering to the ionosphere in the other, the magnetotail, and the solar wind (magnetosheath and cusp/plasma mantle). Due to time variable return from the magnetotail, ions with different routes and energy meet in the inner magnetosphere, making it a zoo of different types of ions in both energy and energy distribution. This zoo is not yet completely entangled, and includes many unanswered phenomena such as mass-dependent energization although the mass-independent drift theory is well justified. Nearly half of heavy ions in this zoo also finally escape to space, mainly due to magnetopause shadowing (overshooting of ion drift beyond the magnetopause) and charge exchange near the mirror altitude where the exospheric neutral density is the highest.

The amount of heavy ions mixing with the solar wind is already the same or larger than that into the magnetotail, and is large enough to directly extract the solar wind kinetic energy in the cusp/plasma mantle through the mass-loading effect and drive the cusp current system. Considering the past solar and solar wind conditions, ion escape might have even influenced the evolution of the terrestrial biosphere.

20

## 1 Introduction

Due to much higher inertia and different cross sections compared to electrons, ion behaviour in the space is less coherent with local fields than electron behaviour. Together with additional complication of specie-dependence, ion phenomena in the magnetosphere is still to be understood. These less understood phenomena include circulation of heavy ions such as oxygen



25 ions  $O^+$ , nitrogen ions  $N^+$ , and molecular nitrogen ions  $N_2^+$  (Chappell et al., 1982; Craven et al., 1985). This paper reviews mainly this circulation part of terrestrial ion based on Bartels Medal lecture at EGU General Assembly 2019, with stress on finding by Cluster and are not covered by review papers on ion circulations (Moore et al., 1999, Blanc et al., 1999, Walker et al., 1999; Ebihara and Ejiri, 2003, Darrouzet et al., 2009; Welling et al., 2015). Since Cluster Ion Spectrometry (CIS) COMposition DISTRIBUTION Function (CODIF) is not design to separate more than four main species  $H^+$ ,  $He^{++}$ ,  $He^+$ , and  
30 atomic ions of the CNO group (Rème et al., 2001), all heavy ions are pedagogically called  $O^+$ , which is the most abundant among heavy ions (Hamilton et al, 1988 et al.; Yau and Whalen, 1992), as is in the conventional manner. The paper is organized as following.

1. Introduction

2. Ion outflow from the ionosphere

35 3. Destinations of the outflow

4. Inner magnetosphere at  $L < 6$ : zoo of many processes

5. Consequences of large amount of direct ion escape

6. Discussion

7. Conclusion

## 40 2 Ion outflow from the ionosphere

Ionospheric heavy ions are found almost everywhere in the magnetosphere (Chappell et al., 1972, Shelley et al., 1972, Hamilton et al., 1988). They are observed even in the high-latitude magnetosheath and plasma mantle (Lundin, 1985, Eklund et al., 1997). Likewise, outflow of ionospheric heavy ions has also been observed (e.g., Moore et al., 1999, André, 2015). There are three types of outflow, which is mainly classified by detection method: (1) cold filling to the plasmasphere (Park, 1974, Welling  
45 et al., 2015), (2) cold supersonic outflow to the inner magnetosphere and magnetotail such as polar wind (Sue et al., 1998; Engwall et al., 2006; 2009), and (3) ions with suprathermal energy above the ionosphere (e.g., Eliasson et al., 1994) or with higher energy at higher altitude (e.g., Möbius et al., 1998).

### 2.1 Cold filling

The cold filling has never been directly detected, but can be estimated from the variation of the plasmasphere (Craven et al.,  
50 1997; Darrouzet et al., 2009; Sandel, 2011, Dandouras et al., 2013). The refilling ions are most likely dominated by thermal  $H^+$  (90% of total density) with secondary population of  $He^+$  (10% of total density). This ratio most likely applies to the refilling flux. The abundance of  $O^+$  is very little but still expected 1-5% of total density, which is much higher than that of the Jeans escape. The refilling mechanism is not yet completely understood (Darrouzet et al., 2009; Gallagher et al., 2016).

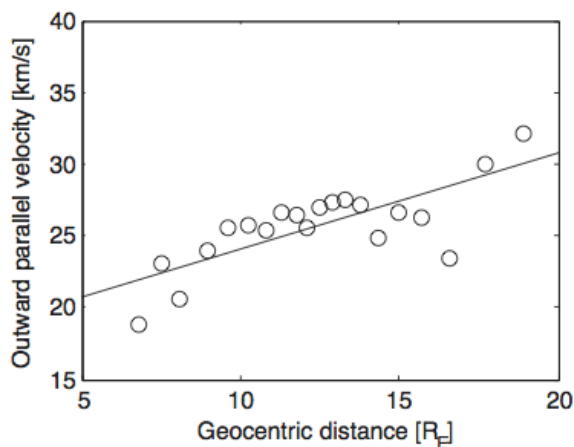


**Figure 1.** Altitude dependence of outward parallel velocity of cold supersonic flow observed by Cluster (Engwall et al., 2009)

## 2.2 Cold supersonic outflow

55 The cold supersonic outflow here means flow of ion with kinetic energy much higher than thermal energy but lower than the satellite potential when it is positive, i.e., inside dense plasma under sunlit (Seki et al., 2003; Engwall et al., 2006). For Cluster case, active potential control did not help detecting it (Sauvaud et al., 2004). Su et al. (1998) tried to supplement such missing ion population at 5000 km altitude, and estimated about 15 km/s upward velocity for  $H^+$  ( $\sim 1.5$  eV) in sunlit without outflowing  $O^+$  (downward motion in average), agreeing with the polar wind mechanism that can cause outflow for only  $H^+$  and  $He^+$  but not  $O^+$ . Engwall et al., (2006) found a new method, although indirect, to obtain the velocity and flux of this cold  
60 supersonic outflow in the lobe region where density is very low. According to this indirect method, typical velocity of these outflowing cold ions at 10–15  $R_E$  from the Earth, i.e., after centrifugal and the other bulk acceleration, is 25 km/s (3 eV) as shown in Fig. 1 (Engwall et al., 2009).

There are many reports of in-situ thermal ion observations (e.g., Pollock et al., 1990; Yau and Whallen, 1992) that claims  
65 polar wind detection (cold supersonic outflow in the present observational terminology), but most of them have high  $O^+$  outflow flux with much higher velocity than this cold supersonic outflow, and they are actually the suprathermal described below, including the apogee observation by Su et al. (1998).

## 2.3 Suprathermal and hot outflows

The last category (suprathermal ions and hot ions) is the one that can be directly detected by the ion instruments. In very few  
70 direct observations that identified both cold supersonic outflow and hot outflow, they are well separated in energy (Olsen, 1992; Seki et al., 2003). The largest sources of these ions in the ionospheric are around the cusp and the auroral oval (Moore et al., 1999; Peterson et al., 2001). In this paper, suprathermal ions and hot ions are not subdivided because the former is further accelerated to become the latter at high-altitudes (Lennartsson et al., 2004; Arvelius et al., 2005; Nilsson et al., 2006) or in

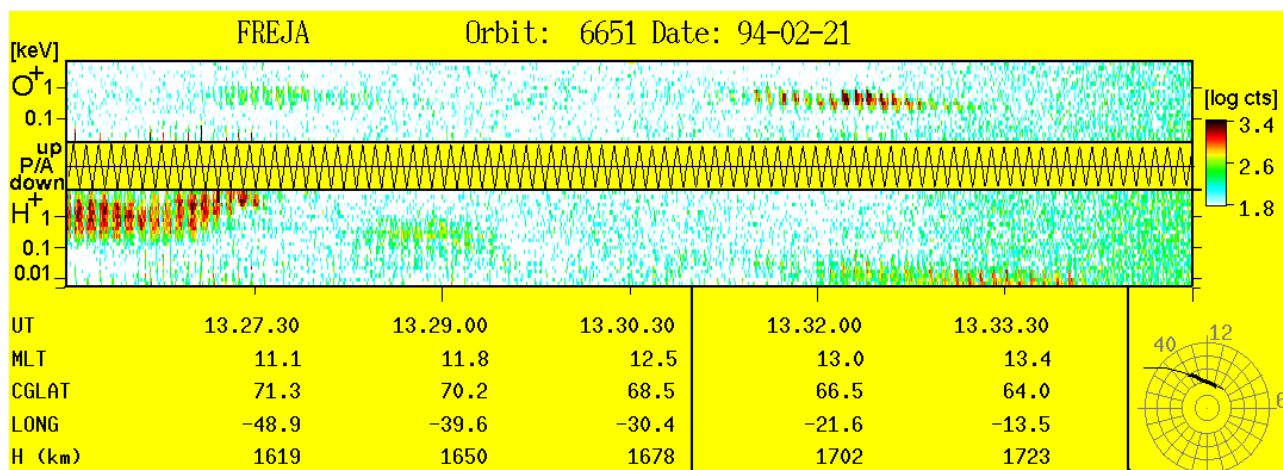


**Figure 2.** Energy-time spectrograms for heavy ions (marked as  $O^+$ ), protons, and electrons on 21 February 1994 observed by Freja in the dayside.  $K_p$  was 7+ and the IMF  $B_Y < -50$  nT, which moved the northern cusp downward and southern cusp duskward (Yamauchi et al., 2005b)

the other hemisphere (Hultqvist, 2002; Yamauchi et al., 2005b). Fig. 2 shows one such example in the dayside observed by Freja during 21 February 1994 magnetic storm event when the interplanetary magnetic field (IMF) was extremely downward (Yamauchi et al., 1996c, 2005b). In such a condition the northern cusp shifts toward prenoon whereas southern cusp shifts toward postnoon, and hence the signature of the southern cusp can be detected in the northern postnoon well separated from the northern cusp signature. Thanks to prenoon-to-postnoon traversal with  $63^\circ$  inclination that is fitted to detect the cusp during substorms, Freja detected cusp-related outflow in both the northern hemisphere as suprathermal ions and the southern hemisphere as injecting hot ions after traveling all the way through the inner magnetosphere. The much higher energy of these injecting ions indicates acceleration during the travel.

One unexpected feature for this event is that the energy ratio between  $O^+$  and  $H^+$  is about 15 when comparing at the same location, and about  $\sim 20$  when comparing the energies of most intense injections. This indicates that they have the same velocity rather than the same energy even after considering the possible velocity filter effect (ions with the same field-aligned velocity arrives at the same location under substantial perpendicular convection). Cluster statistics of the hot outflowing ions at high-altitude polar region also shows that energization is toward the same velocity rather than the same energy (Nilsson et al., 2006). Polar apogee observation at  $8 R_E$ , which is normally in the polar cap, showed the ratio of field-aligned bulk velocity between  $O^+$  and  $H^+$  ( $V_{O\parallel}/V_{H\parallel}$ ) about 0.3-0.6 (Su et al., 1998). However, the value is underestimated because the upper energy threshold of the instrument was 350 eV ( $\sim 60$  km/s for  $O^+$ ), whereas Cluster statistics that showed that more than half the  $O^+$  outflow events at that altitude had energy higher than 350 eV (Arvelius et al., 2005). Nevertheless, the result is larger than 0.25 that corresponds to the same energy.

These observations indicate that the energization of the dayside hot ion outflow at mid- and high-altitudes are mainly by waves or other non-thermal processes (Moore et al., 1999; Lennartsson et al., 2004; Waara et al., 2011). This applies even at

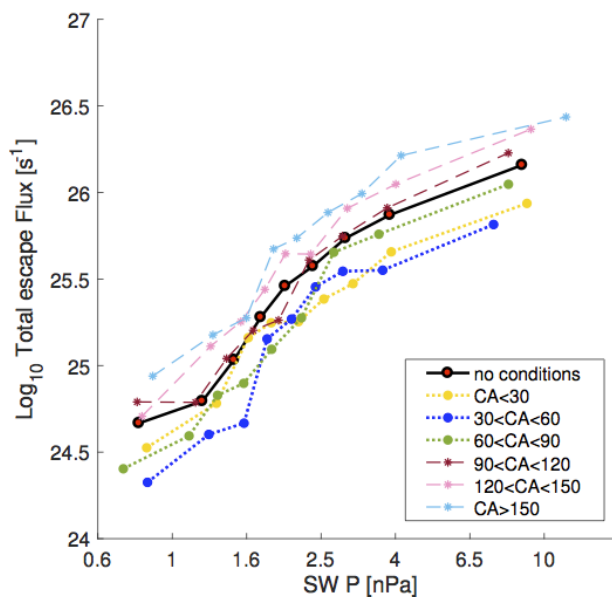


**Figure 3.** Cluster statistics of hot heavy ions ( $O^+$ ) escape to the space at the plasma mantle and magnetosheath. Total escape flux of the heavy ions is plotted as a function of the solar wind dynamic pressure for different IMF clock angle (CA), which is defined as  $0^\circ$  for northward IMF (Schillings et al, 2019)

low-altitudes because majority of the dayside outflowing ions at low altitudes are conic-like at low altitude rather than beam  
95 like (Norqvist et al., 1996; Peterson et al., 2008). On the other hand, a substantial part of nightside outflow is in the beam  
form (Norqvist et al., 1998; Peterson et al., 2008), after most likely accelerated by parallel electric potential above the discrete  
aurora. In a such case, we expect  $V_{O\parallel}/V_{H\parallel} = 0.25$  and hence  $O^+$  moving more downstream than  $H^+$  compared to mapping  
location along the geomagnetic field due to the velocity filter effect.

For the composition, satellite observations of the suprathermal and hot ions showed a higher outflow flux for  $O^+$  than  $He^+$ .  
100 This again indicates non-thermal energization mechanisms. The outflowing flux ratio between  $O^+$  and  $H^+$  ( $F_O/F_H$ ) is about  
0.1 for suprathermal energy range (thermal ion instrument for  $< 50$  eV) and is close to 1 for hot ion energy range of  $>$  few eV  
up to tens keV (Moore et al., 1999; Curry et al., 2003; Peterson et al., 2001; Sandhu et al., 2016). Similar difference is also  
found on the solar EUV effect (not solar zenith angle but F10.7) between the suprathermal ion observation by Akebono (Cully  
et al., 2003) and the hot ion observation by Cluster (Schillings et al., 2019). The former showed more than one order magnitude  
105 increase of outflow flux for  $O^+$  with very little increase for  $H^+$ . The latter showed almost no increase of  $O^+$  outflow flux for  
different EUV flux as shown in Fig. 3a.

These differences can be explained by upper energy threshold of suprathermal ion instrument because the energization is  
rather toward the same velocity than same energy between  $O^+$  and  $H^+$ . This makes  $O^+$  outside the upper energy threshold  
of the suprathermal ion instrument. In other words, one may not treat the suprathermal ions differently from the hot ions,  
110 but differently from cold supersonic flow (polar wind in the modelling terminology). The same logic may apply to the lower



energy threshold for the hot ion instrument if the observation is low-altitude ( $< 2 R_E$ ) where  $H^+$  are not sufficiently energized for detection (e.g., Peterson et al., 2001). On the other hand, Cluster altitude is high enough for suprathermal ions sufficiently accelerated, while cold supersonic outflow are still  $< 5$  eV, as mentioned above. For the EUV effect, the  $O^+$  enhancement for high EUV can be explained by the enhanced number density without extra energy for non-thermal energization at higher altitudes requires the solar wind energy input. In fact, response of the ionospheric density and ion outflow to the 6-8 September 2017 event showed density enhancement after X9.3 flare without enhancement of ion outflow, which increase after the arrival of solar energetic particle event or coronal mass ejection (Yamauchi et al., 2018). Therefore, we do not need to introduce new energization mechanisms to explain the  $O^+/H^+$  ratio difference at different energy ranges and altitudes.

### 3 Destinations of the outflow

This section describes immediate destinations but not the final destinations.

#### 3.1 Cold filling to plasmasphere

The destination of cold filling is mainly the plasmasphere as mentioned in Section 2.1. The refilling rate is estimated from the recovery of plasmasphere after losing massive amount of cold ions as the plasmaspheric plumes (Sandel and Denton, 2007; Darrouzet et al., 2008) or outward wind (Dandouras et al., 2013) because these loss are most likely lost to the space rather than returning.

#### 3.2 Known destination for cold supersonic outflow

The destination of the cold supersonic outflow is not yet clear except the tail plasma sheet because the measurement is possible only in the low-density lobe region (Engwall et al., 2006; André, 2015). Since the observation is not easy, we have no knowledge on the other possible destinations. Engwall et al. (2009) derived the total flux flowing in the lobe and its Kp dependency and solar wind dependency. Their results can be scaled to roughly  $3 \exp(0.23Kp) \times 10^{25} \text{ s}^{-1}$  for  $H^+$ , with very low ( $\leq 1\%$ )  $O^+/H^+$  ratio.

In the lobe, the plasma convection across the geomagnetic field cannot be ignored compared to the outflow velocity, making the velocity filter effect between  $H^+$  and  $He^+$  significant (Chappell et al., 1987) unless the acceleration is to exactly the same velocity for different masses. If the Polar observation at 5000 km altitude by Su et al. (1998) corresponds to this outflow, we expect different outflow velocity between  $H^+$  and  $He^+$  although their observation is only for  $H^+$  and  $O^+$  but not  $He^+$ . In this case,  $H^+$  will reach further distance than  $He^+$  in the tail plasma sheet.

#### 3.3 Various destinations for hot outflow

For the suprathermal and hot ions, the destination depends on the starting location and condition in the ionosphere. The dayside outflow has wide destination ranging the tail plasma sheet, the plasma mantle, and even the magnetosheath (Shelley et al., 1972;

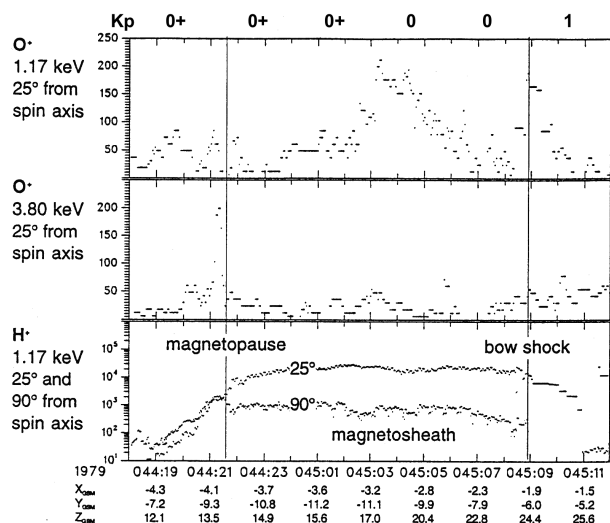


**Figure 4.** Prognoz-7 ion composition data in the dayside magnetosheath on 13 February, 1979 (Eklund et al., 1997). Ionospheric ions are observed in the magnetosheath even during prolonged period of low geomagnetic activity with Kp=0.

140 Lundin 1985; Slapak et al., 2017a, b). Fig. 4 shows one such example in the magnetosheath and plasma mantle (Eklund et al., 1997).

Among these immediate destinations, direct loss to the space through the plasma mantle and magnetosheath has been underestimated before the Cluster observations. Thank to its high inclination highly elliptic orbit with large apogee distance (Polar apogee was not sufficient for such study) and proper instrumentation, Cluster could make statistics over high-latitude magnetospheric boundary region. The total hot O<sup>+</sup> flux into plasma mantle and magnetosheath is as large as 10<sup>25–26</sup> s<sup>-1</sup> (Nilsson et al., 2012; Slapak et al., 2017a) and is larger than the total hot O<sup>+</sup> flux into the tail plasma sheet (Slapak et al., 2017b, Slapak and Nilsson, 2018). Geotail found mantle-like population in the distant-tail plasma sheet beyond X < -150 R<sub>E</sub> (Maezawa and Hori, 1998). They are flowing anti-sunward, supporting that mantle flow is generally lost to the space. The plasma mantle and magnetosheath are thus significant as the destination.

150 The outflowing ions from the nightside ionosphere, particularly for O<sup>+</sup> when the velocity filter effect is considered, may flow into the inner magnetosphere and reach the other hemisphere as mentioned above (Cattell et al., 2002; Hultqvist, 2002; Yamauchi et al., 2005b). If ions are accelerated by the parallel electric potential drops, they may reach the other ionosphere. In fact, Freja at 1700 km altitude detected injecting ions with similar energy between H<sup>+</sup> and O<sup>+</sup> (V<sub>O||</sub>/V<sub>H||</sub> ~ 4) in keV range, suggesting that they are accelerated by parallel electric potential (Hultqvist, 2002). This injecting ions also indicates the velocity filter effect: the O<sup>+</sup> injection events are found mostly inside or equatorward of what traditionally called the central plasma sheet (CPS), region of thermal unstructured electrons at several keV range (Winningham et al., 1975; Woch and Lundin, 1993), and at equatorward of the H<sup>+</sup> injection events that are found in the entire auroral zone (Yamauchi et al., 2005b).



However, outflowing ions starting from conic, which normally have lower parallel velocity and higher perpendicular velocity than ion beams, is expected to be mirrored and trapped in the inner magnetosphere as mentioned in Section 2.3. In fact, the inflow flux is much smaller than expected. Freja detected only about 50 O<sup>+</sup> clear injection events over more than 5000 traversals over the auroral oval (Yamauchi et al., 2005b). For H<sup>+</sup>, statistics of DMSP at 840 km altitude of ion inflow (mainly H<sup>+</sup>) shows 1-2 order magnitude smaller flux than outflow flux including the cusp (Hardy et al., 1989; Peterson et al., 2008; Newell et al., 2010), and this difference is larger in the nightside. Thus, majority of the suprathermal and hot ions outflowing toward the other hemisphere via the inner magnetosphere are not entering the ionosphere, but rather start bouncing (Quinn and McIlwain, 1979; Hiraraha et al., 1997).

### 3.4 Secondary destinations from the near-Earth tail

A significant flux of ions enters the near-Earth tail plasma sheet ( $-10 R_E < X < -20 R_E$ ) as the primary destination for both the cold supersonic outflow (Engwall et al., 2009; André, 2015) and the suprathermal/hot outflow (Sauvaud et al., 2004; Maggiolo and Kistler, 2014; Slapak et al., 2017b). This makes the plasma sheet a mixture of time-variable terrestrial ions into relatively stable solar wind ions, including the O<sup>+</sup>/H<sup>+</sup> ratio for terrestrial ions and the He<sup>++</sup>/H<sup>+</sup> ratio for the solar wind (Lennartsson, 1997, 2001; Nosé et al., 2009). Some of these terrestrial ions keep flowing anti-sunward, particularly those which has large anti-sunward velocity along the geomagnetic field. The rest of the terrestrial ions in this region returns to the Earth as either slow convection or bursty flows (Ohtani et al., 2004; Slapak and Nilsson, 2018), with higher He<sup>++</sup>/O<sup>+</sup> ratio than the anti-sunward flow that are lost to the space (Lennartsson, 2001).

Using Cluster hot ion composition data (covering  $> 28$  eV), Slapak et al. (2017b) derived the total sunward (Earthward) and anti-sunward fluxes in the plasma sheet at  $X \sim -10 R_E$  (they actually used the Cluster crossing between  $-20 R_E$  and  $-10 R_E$ ), for both H<sup>+</sup> and O<sup>+</sup>, respectively. Slapak and Nilsson (2018) further examined O<sup>+</sup> flux in the lobe. The average net flux (budget) of hot O<sup>+</sup> in the nightside magnetosphere (lobe and plasma sheet) is  $1 \times 10^{24} \text{ s}^{-1}$  in the anti-sunward direction as the result of high return rate ( $6 \times 10^{24} \text{ s}^{-1}$  out of  $7 \times 10^{24} \text{ s}^{-1}$  anti-sunward flux). A complete result with Kp dependence is summarized in Table 1, where the average value corresponds approximately to Kp=3, which gives the exponential factor as about 3.3-3.9. The escaping amount through the tail plasma sheet is one order of smaller than that through plasma mantle and magnetosheath (Slapak et al., 2017a, Schillings et al., 2019).

The Cluster result of the O<sup>+</sup> return flux near the Earth is smaller than indirect "guess" by Seki et al. (2001), who estimated the return flux only from decrease of anti-sunward hot ion flux with distance, by using an ion instrument without mass separation with upper energy limit of only 17 keV from Geotail. In addition to the orbital limitation to equator, O<sup>+</sup> has wide energy around the solar wind speed (450 km/s for 17 keV O<sup>+</sup>) at the distant tail, as was demonstrated for the downstream of Venus (Grünwaldt et al., 1997), and hence instrument missed majority O<sup>+</sup> escape flux during fast solar wind conditions, i.e., when the escape flux is high (Schillings et al., 2017, 2019).

The return rate compared to detectable anti-sunward flow in the plasma sheet is much higher for H<sup>+</sup> (earthward  $1.3 \times 10^{26} \text{ s}^{-1}$  with visible anti-sunward  $5 \times 10^{25} \text{ s}^{-1}$ ) than O<sup>+</sup> (Lennartsson, 2001; Slapak et al., 2017b), supporting the extremely low O<sup>+</sup>/H<sup>+</sup> ratio for the hidden cold supersonic flow. In other words, we may safely ignore O<sup>+</sup> in the cold supersonic flow into



**Table 1.** Major outflow destinations and flux of O<sup>+</sup> observed by Cluster

primary destination	Fig. 6	energy	average ( $\times 10^{25} \text{ s}^{-1}$ )	range ( $\times 10^{25} \text{ s}^{-1}$ )	escape?
magnetosheath	(d)	0.03-40 keV <sup>*1</sup>	0.7	0.14 exp(0.45Kp)	all
plasma mantle	(d)	0.03-40 keV <sup>*1</sup>	2	0.82 exp(0.45Kp)	mostly
lobe	(c)	0.03-40 keV <sup>*2</sup>	0.3	0.07 exp(0.43Kp)	>half
lobe	(c)	supersonic <sup>*3</sup>	(< 0.1)	< 0.03 exp(0.23Kp)	>half
magnetotail (tailward)	(c)	0.03-40 keV <sup>*2</sup>	0.5	0.15 exp(0.40Kp)	all
magnetotail (earthward)	(c)	0.03-40 keV <sup>*2</sup>	0.6	0.18 exp(0.42Kp)	half
inner magnetosphere	(b)		small		half
plasmasphere	(a)	cold	<1.8 <sup>*4</sup>		mostly

\*1 Slapak et al. (2017a), \*2 Slapak and Nilsson (2018), \*3 Engwall et al. (2009), \*4 Upper limit without direct O<sup>+</sup> observations.

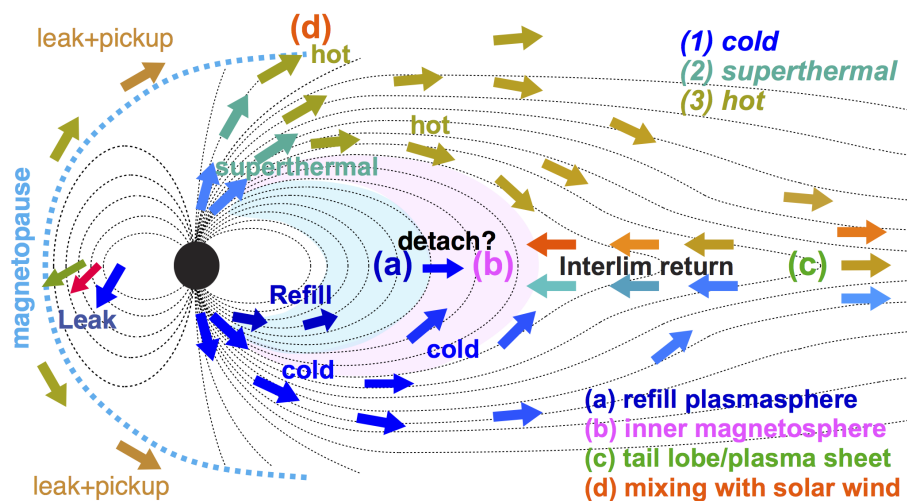


**Figure 5.** Summary of the destinations of ion outflow

the plasma sheet when discussing the total amount of escape and return, although Slapak et al. (2017b) and Slapak and Nilsson (2018) could not include such hidden flow (covering O<sup>+</sup> with returning velocity of > 60 km/s only). Destinations of different type of outflowing ions are summarized in Fig. 5.

195 Once the ionospheric ions enter the plasma sheet, they are energized by heating (Sergeev et al., 1993; Lennartsson, 1997; Kistler et al., 2005) and  $\mathbf{J} \times \mathbf{B}$  force (Walker et al., 1999; Ohtani et al., 2004). Even the cold ions are heated to  $\sim 100$  eV according to both the direct and indirect case studies (Seki et al., 2003; Ebihara et al., 2008). Furthermore, ions returning to the Earth in the plasma sheet undergo adiabatic energization (Alfvén and Fälthammar, 1963; Blanc et al., 1999). In this way, cold ions in the plasma sheet gain sufficient energy to detect with hot ion instruments in the inner magnetosphere at a different  
 200 energy range from the hot component. As the result, ion injection from the tail plasma sheet covers a wide energy range at wide



latitudes as shown in Fig. 6a. Still it is possible to separate two components because of different temporal variations between the cold source and hot source. In fact, particle drift simulations reproduced the dual populations observed ("warm" <100 eV component and "hot" few keV component) by satellites (Ebihara et al., 2008; Yamauchi et al., 2009a). They also showed that the cold-origin warm component varies in time much more than hot plasma sheet component, as is described in more detail in  
205 the next section. As the result, latitude-energy distribution of ions varies with MLT as shown in Fig. 6. In the figure, north-south symmetric morphologies come from Cluster orbit because it traversed the inner magnetosphere from the southern hemisphere to the northern hemisphere along the same longitude within 1-2 hours in a symmetric manner during 2001-2006.

#### 4 Inner magnetosphere at $L < 6$ : zoo of many processes

As illustrated in Fig. 5, all types of outflow may enter the inner magnetosphere directly or indirectly, making the inner mag-  
210 netosphere a convolution of different ions. Among those, ion population and dynamics in the inner magnetosphere with only one or two sources has well studied long, with good reviews for cold plasmaspheric ions (Darrouzet et al., 2009), ordinary ring current ions at  $> 10$  keV (Daglis et al., 1999), radiation belt (Blanc et al., 1999), and theories (Ebihara and Ejiri, 2003). However, sources and dynamics of hot sub-keV ions has been less understood, partly because ions in this energy range has many different sources. This paper mainly review this energy range.

215 The hot ion source is not only from the plasma sheet, but can directly be supplied from the ionosphere, as mentioned in Section 3.3. Horwitz and Chappell (1979) found field-aligned "warm" ions of about 10 eV temperature with small bulk velocity in the inner magnetosphere and its high-temperature cases are also observed by Cluster (Yamauchi et al., 2013). Local heating of the cold ions, particularly in the equatorial plane can also produce hot ions from the cold plasmaspheric ions (Olson et al., 1987). Combining with, the inner magnetosphere becomes rich in various types of sub-keV ions (Yamauchi et al., 2013).  
220 Figs. 7-9 show some examples observed by Cluster (Yamauchi et al., 2006a, 2009b, 2014a).

Such convolution of sources is one of the reason why the formation mechanisms for these sub-keV ions in the inner magnetosphere were not well studied, particularly the region within geosynchronous orbit or  $L < 6$  ( $L$  is the distance to the geomagnetic field that is measured at the equator in the unit of Earth radius  $R_E$ ), although many magnetospheric missions 50-30 years ago already detected these ions (Sauvaud et al., 1981; Chappell et al., 1982; Newell and Meng, 1986; Yamauchi et al., 1996a,  
225 2006a). This restrictive ( $L < 6$  or invariant latitude ( $Inv < 65^\circ$ )) region is called as "inner magnetosphere" in this paper.

##### 4.1 Energy-dependency of ion drift

To de-convolute different sources and mechanisms, prediction of morphologies from all the known sources using ion drift simulation is useful because ion motions in the inner magnetosphere are, thanks to the strong geomagnetic field, basically dominated by magnetic (gradient-B and curvature) drift and the  $E \times B$  drift. The magnetic drift (velocity  $V_B$ ) moves ions  
230 westward in nearly constant in time but in an energy-dependent manner. For example, for ion energy ( $W$ ) in dipole field (strength at equator  $B$ ), it is approximately

$$V_B \propto \frac{g(\alpha) \cdot W}{B \cdot L} \quad (1)$$



### Cluster (SC-4) CIS/CODIF data

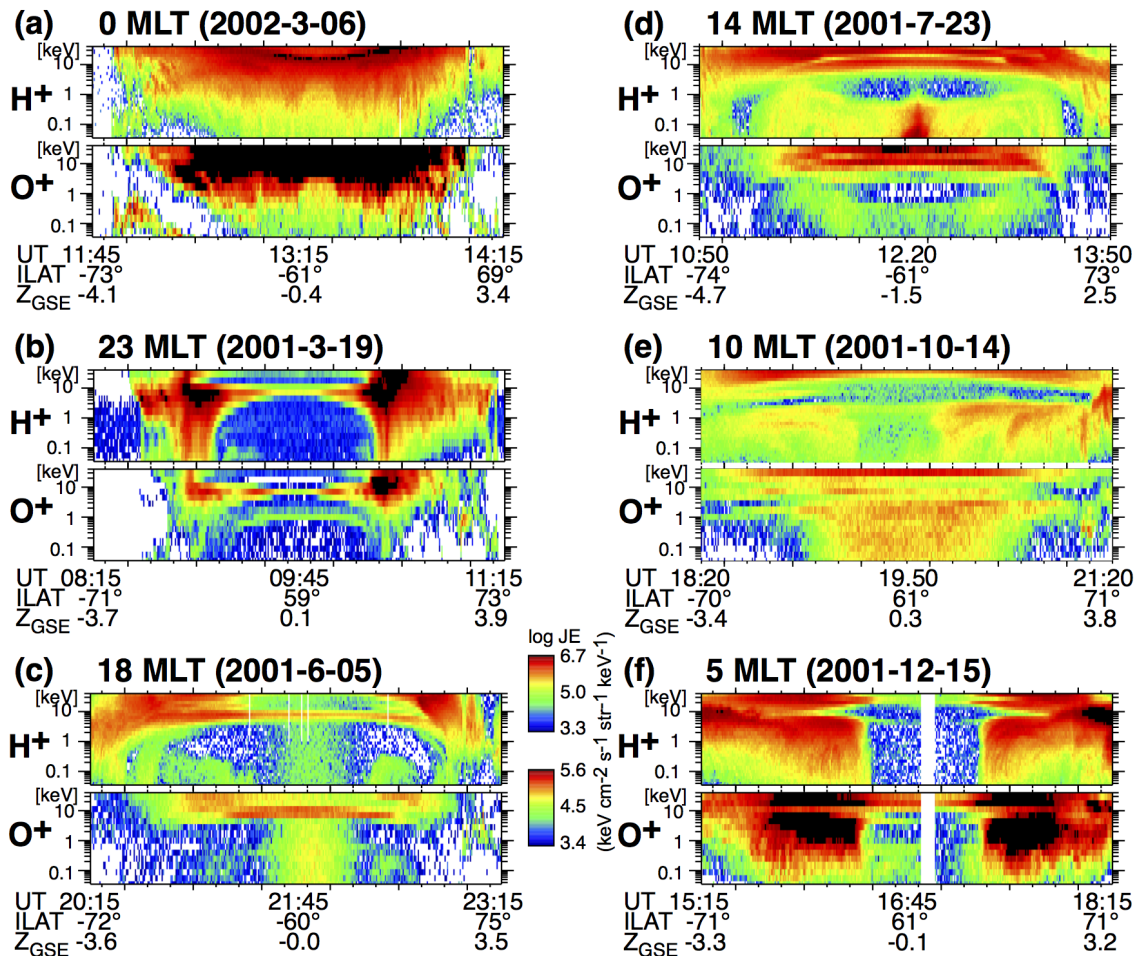


**Figure 6.** Cluster examples of the energy-time spectrograms of hot ion differential energy fluxes ( $\text{keV cm}^{-2} \text{s}^{-1} \text{str}^{-1} \text{keV}^{-1}$ ) at different local times in the inner magnetosphere before and after its perigee (nearly  $4 R_E$ ). The heavy ions (marked as  $\text{O}^+$ ) eventually includes all CNO group ions. Orbit during these observations are nearly north-south symmetric along nearly the same local time starting from the southern hemisphere.

where the factor  $g(\alpha)$  is 2 for pitch angle  $\alpha = 0^\circ$  and 3 for  $\alpha = 90^\circ$ . Contrary, the  $E \times B$  drift varies in time although it is energy independent, with its velocity ( $V_E$ ) proportional to  $E/B$  where  $E = E(t)$  is the electric field component perpendicular to magnetic field. The  $E \times B$  drift moves ions eastward during quiet time (co-rotation), but sunward drift component (westward in the dusk and eastward in the dawn) is added by externally driven dawn-to-dusk electric field during active period. This motion is dominant for cold plasmaspheric ions that have zero magnetic drift velocity (Goldstein, 2006; Darrouzet et al., 2008). Both drifts are mass independent, i.e., the drift velocity is the same if the energy is the same.

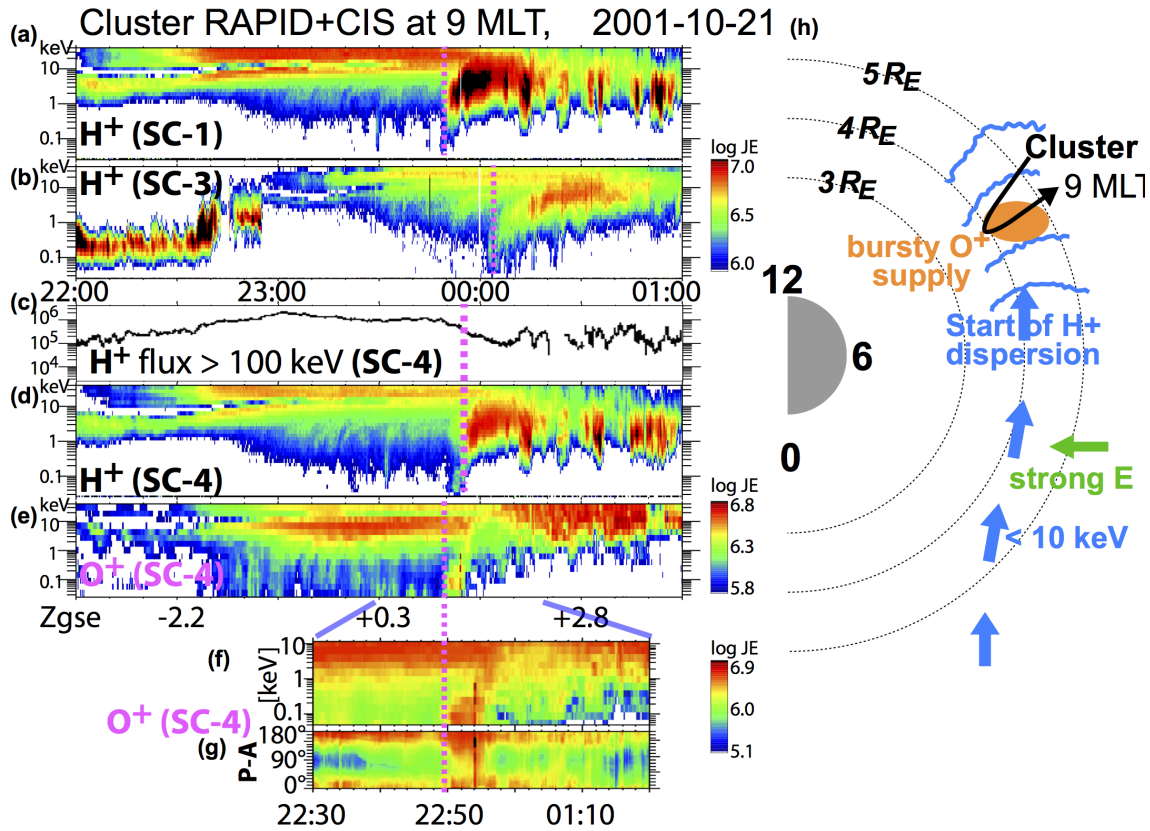


**Figure 7.** Summary of the Cluster observation and its interpretation of the sudden appearance of hot ions starting at around 21:50 UT on 21 October 2001 (Yamauchi et al., 2006a). Left: Energy-time spectrograms of differential energy fluxes (keV cm<sup>-2</sup> s<sup>-1</sup> str<sup>-1</sup> keV<sup>-1</sup>) for protons from (a) spacecraft (SC)-1, (b) SC-3, and (d) SC-4 and (e) for heavy ions (O<sup>+</sup>) from SC-4. For SC-4, (d) energetic proton flux is also plotted. Bottom panels show (f) a zoom up of (e), and (g) energy-pitch angle spectrograms of the same data.

Adding both the magnetic and  $E \times B$  drifts, westward ion drift is expected for high energy (generally > 20 keV; so called ring current) or in the evening sector, and eastward for low energy (generally > 5 keV) and in the morning sector. The combination of these drifts also adiabatically energizes ions through the conservation of adiabatic invariant as

$$\frac{W}{W_0} = \left(\frac{L}{L_0}\right)^{-g(\alpha)} \quad (2)$$

where suffix 0 denotes initial energy and location (Ejiri, 1978). Assuming a dipole field ( $B \propto L^{-3}$ ),  $V_B$  is larger for larger  $L$ , particularly for high  $\alpha$ .

Using simple dipole field and dawn-dusk symmetric electric field, Ejiri et al. (1980) simulated the drift motion starting from 10  $R_E$  and re-constructed energy- $L$  spectrogram of virtual satellite observation over  $L=2-6$  for both ions and electrons. In their simulation, nose-like diminishing of the westward drifting ions toward the lower latitude (nose structure) and boundary of the

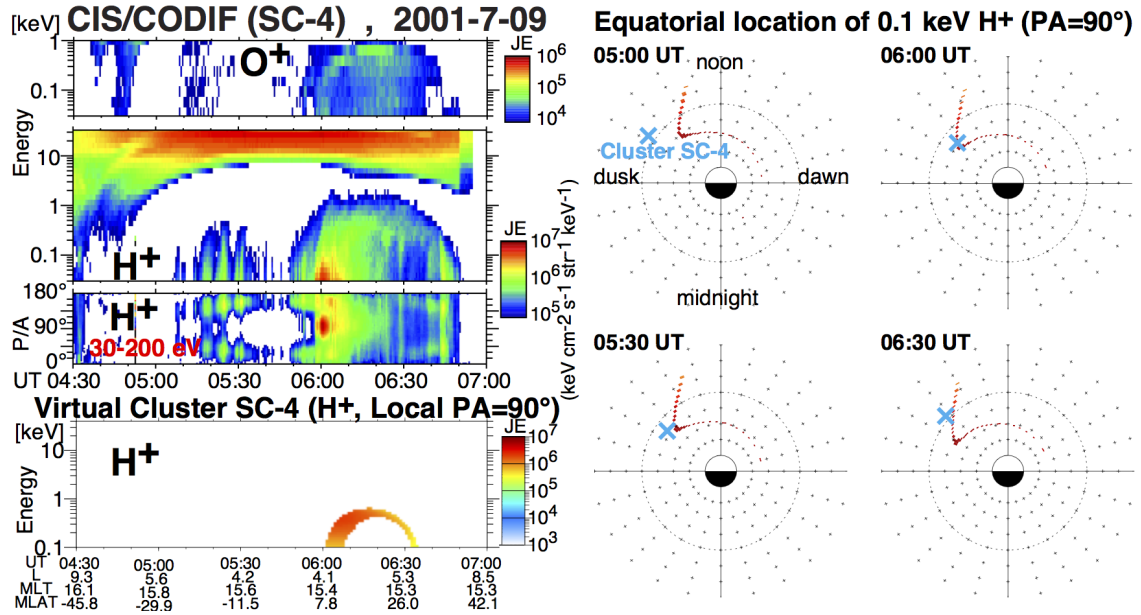


**Figure 8.** Cluster CODIF perigee observation on 9 July 2001 and its ion drift simulation using Volland-Stern electric field model (Yamauchi et al., 2014b). Three types of sub-keV ions (eastward drifting energy range) are convoluted in the ion data (i) recently injected nearly field-aligned suprathermal ions during 05:15-05:35 UT, (ii) equatorially-trapped perpendicularly heated plasmasheric ion at 05:59-06:02 UT, and (iii) arch-like dispersed ions during 05:50-06:50 UT. The first one was observed at the similar timing between SC4 and SC3 whereas the second one was observed at the local equator that is 30 min apart between SC4 and SC3. The simulation in the bottom panel reproduced only the last type. Locations of the simulated 0.1 keV  $H^+$  and Cluster was shown in the right panel.

forbidden region for the eastward drifting ions are qualitatively reproduced at 5-10 hours after the start of injection. Examples of the nose structure are shown Figs. 6b and 6c ( $H^+$  10 keV band), and examples of forbidden region are shown in Figs. 6d-6f (< 5 keV ions).

At energy between the westward and eastward drift regimes, we expect no ion population (Collin et al., 1993; Jordanova et al., 1999). This "gap" energy is estimated by setting the ratio of azimuthal drift velocities

$$\left(\frac{V_E}{V_B}\right)_\phi \sim \frac{6.6 \cdot L \cdot E_r [\text{mV/m}]}{g(\alpha) \cdot W [\text{keV}]} \quad (3)$$

as unity, where  $E_r$  is the radial (duskward in the dawn sector) electric field (Yamauchi et al., 2006a). To have a new injection from the magnetotail, we need a duskward external electric field, during which the inward electric field  $-E_r$  decreases with increasing local time starting from the dusk sector, making  $W_{gap}$  also decreasing, as seen in Fig. 6. Such a local-time dependence is statistically confirmed by Viking and Cluster (Yamauchi and Lundin, 2006, Yamauchi et al., 2006a).

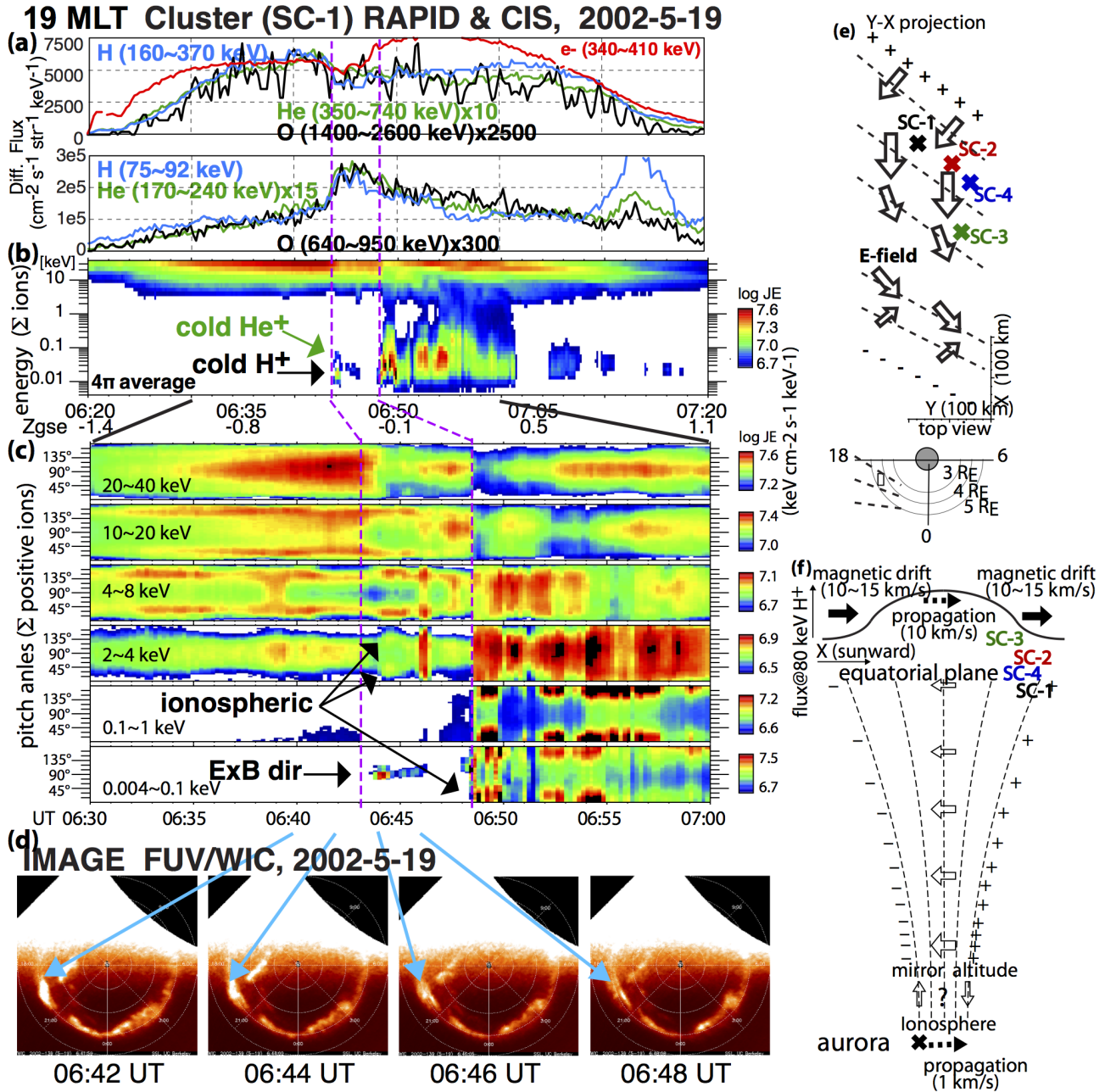


**Figure 9.** Summary of (a) Cluster energetic ion flux, (b) hot ion energy-time spectrograms and (c) energy-pitch angle spectrograms of differential energy fluxes (keV cm<sup>-2</sup>s<sup>-1</sup>str<sup>-1</sup>keV<sup>-1</sup>), (d) IMAGE observations, and (e) interpretation of ion behavior at around 06:43 UT on 19 Mays 2002 (Yamauchi et al., 2009b). These ion at the equator that is conjugate with westward auroral bulge are interpreted as a sunward propagation of high-amplitude DC electric field accompanied by polarization.



## 4.2 Dynamics of cold plasmaspheric ions

For plasmaspheric dynamics, readers may refer to the review by Darrouzet et al., (2009). Here is some extra note from a view-  
260 point of low-energy extreme of hot ions. Since the magnetic drift velocity is zero for cold ions, majority of the plasmaspheric  
ions move according to time dependent  $E \times B$  drift which is a summation of convection by the external electric field and the  
co-rotation. A sudden enhancement of duskward external electric field adds an inward motion in the midnight sector and out-  
ward motion added in the noon sector. As the result of such a pumping force, the plasmasphere is eroded in the nightside and  
plume is formed in the dayside, as have been reported half century ago. However, overall plasmaspheric dynamics (including  
265 erosion, plume formation, its detachment, and even smaller structures) has not been synthesized until IMAGE FUV succeeded  
to take "photograph" of the plasmaspheric  $\text{He}^+$  (Goldstein, 2006, Darrouzet et al., 2009). The detachment starts near the noon,  
with the outer part reaching the magnetopause and escaping to the magnetosheath (called as magnetopause shadowing) in the  
entire afternoon sector, as is also confirmed with plasma wave data (Darrouzet et al., 2008), while rest of plume might detach  
in the nightside. This agrees with the local time dependence of the demarcation energy between westward drift and eastward  
270 drift as mentioned above.

In addition to these cold ion dynamics, ions are often heated in the perpendicular direction to the magnetic field near the  
equatorial plasmopause within a few degree latitudinal range (Olsen, 1987). These equatorially-trapped warm ions are observed  
during nearly all geomagnetic conditions, and are mainly found at  $< 5 R_E$  at all local times, i.e., in the outer part of plasmasphere  
(Darrouzet et al., 2009). The development time is estimated about 1 hour but it decays before drifting over few hours in local  
275 time. Fig. 10 shows one such example observed by Cluster (Yamauchi et al., 2012). Just limiting to the geocentric distance that  
Cluster traversed ( $4.0-4.5 R_E$  at equator) and to ions more than 30 eV (strong heating), these ions are found nearly half the  
noon-dusk traversals during solar maximum, while probability is slightly lower in the night-dawn traversals because these ions  
are normally found at shorter geocentric distance there. The upper energy is normally  $< 100$  eV for  $\text{H}^+$  and  $< 500$  eV for  $\text{He}^+$   
with variable  $\text{He}^+/\text{H}^+$  ratio for both energy (1-5) and density (0-10%). In Fig. 10, both  $\text{He}^+$  and  $\text{H}^+$  show ring distribution  
280 with nearly  $90^\circ$  pitch angles, while simple pancake distribution with nearly  $90^\circ$  pitch angles is more commonly observed,  
particularly for  $\text{H}^+$ , indicating two-step energization mechanisms for ring distribution. The wave modes that is responsible for  
such energization has not been identified.

## 4.3 Dynamics of hot ions injecting from tail plasma sheet

Before examining outflowing ions directly reaching from the ionosphere to the inner magnetosphere, we consider hot ions  
285 injecting from the tail plasma sheet. The basic motion of these injecting ions is described in Section 4.1, but the actual direction  
of the drift (westward or eastward) depends on the start energy and  $Y$  location. The injecting ions have wide energy range when  
they arrive at edge of the inner magnetosphere ( $L=6$  in this paper) because degree of the adiabatic energization depends on  
the start location in both dawn-dusk ( $Y$ ) direction and anti-sunward ( $-X$ ) direction (Ejiri, 1978; Ebihara and Ejiri, 2003). In  
addition, externally driven electric field varies much faster than the drift time over few hours in local time, making the injection  
290 time to a certain L-shell energy dependent and varying in time. This situation can be approximated by multiple injections.

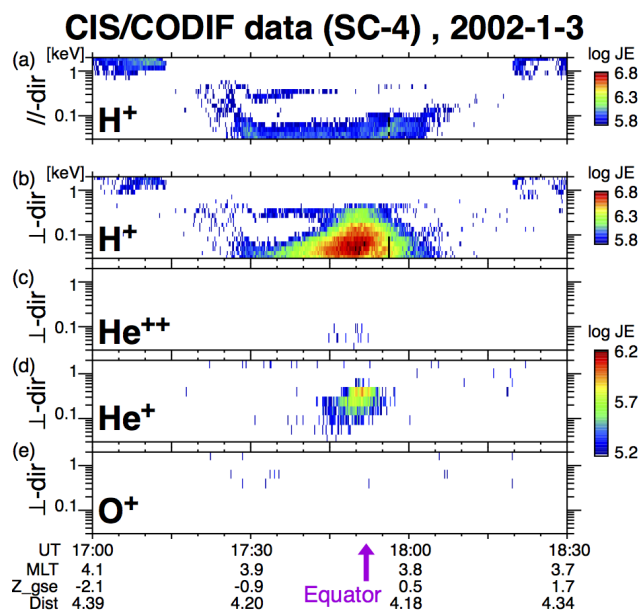


**Figure 10.** Cluster hot ion energy-time spectrograms of differential energy fluxes ( $\text{keV cm}^{-2} \text{s}^{-1} \text{str}^{-1} \text{keV}^{-1}$ ) during perigee traversal on 3 January 2002 (Yamauchi et al., 2012). The most field-aligned sector and the most perpendicular sectors to the geomagnetic field are plotted. The vertical arrow at the bottom indicates the crossing of the equatorial plane that is identified by the wave activity observed by WHISPER.

Since ions at different energy has different drift velocities on the same L-shell, ions at higher energy arriving the same L-shell later than previously arrived ions overtakes. The local time of such overtaking depends on L and the electric field.

Such multiple bands of westward drifting ions are indeed observed (Ebihara et al., 2004; Vallet et al., 2007), like Figs. 6b-6d at around 10 keV and above 30 keV. When the injecting flux is very large (e.g., during major magnetic storms), the westward drift of high-energy ions ( $> 10$  keV) is fast enough to make more than one round of the Earth before decaying, causing another type of multiple band at the same L shell, but that is not as often as electron that drifts around the Earth much faster than ions.

Contrary to westward drifting ions, eastward drifting ions occupy rather wide energy range because the  $E \times B$  drift is energy independent. Since the externally driven electric field varies with short time scales compared to the drifting time scale as mentioned above, the morphology of eastward drifting ions significantly varies in time, as shown in (Figs. 7-9). As the result, the demarcation energy depends strongly on the external electric field and hence the substorm activity. For sever substorms, even ions  $> 40$  keV may drift eastward at  $L=4-5$  (Yamauchi et al., 2009a).

Overlaying these band structures, we sometimes see vertical stripes with wedge-like energy-latitude dispersion at energies below the westward drifting band ("wedge-like structure") in the energy-time spectrogram like Figs. 7 and 11. These vertical stripes with more or less dispersion are found mainly from the midnight to morning sectors. Sometimes, the westward drifting band also ends with similar wedge-like structure, particularly in the noon to afternoon sectors.

The energy-latitude dispersion comes from L-dependence of drift velocity for both magnetic and  $E \times B$  drifts through the strength and curvature of magnetic field (cf. Eq. (3) for part of this L-dependence), as shown in Fig. 8 for 0.1 keV ions. In

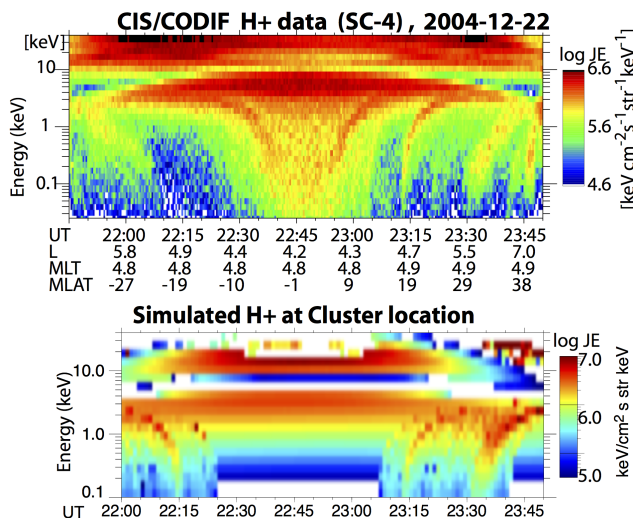


**Figure 11.** Energy-time spectrograms of ion differential energy flux during perigee traversal of Cluster SC-4 on 22 December 2004, and re-construction of energy-time spectrogram by particle drift simulation (Yamauchi et al., 2009a). The simulation shows dual populations ("sub-keV" and "hot" components) with sub-keV component varying in time much more than hot component. The ion signatures that are not re-constructed have different source from the tail plasma sheet (see text).

observations, there are three different dispersion patterns of these wedge-like structures (Yamauchi et al., 1996a; Ebihara et al., 2001; Yamauchi et al., 2005a): increasing energy with L like Figs. 6e and 11, decreasing energy with L like Fig. 6d, and first  
 310 increasing and then decreasing energy with L like Figs. 6c and 8. All patterns have been reproduced by a combination of ion drift simulation and phase-space mapping (Ebihara et al., 2001). A single simulation can also reproduce both eastward drifting components (band and the wedge-like structure), as shown in Fig. 11.

Since the electric field in the inner magnetosphere can be modelled (Ebihara, 2003; and references therein), one can even estimate the original energy distribution at the start location. The simulation indicates that these ions most likely originate from  
 315 low-energy ions with temperature < 100 eV), i.e., ions supplied as cold supersonic flow as mentioned in Section 3.2 (Ebihara et al., 2008; Yamauchi et al., 2009a). The duration of each stripe corresponds to duration of the supply of these "cold" ions. The result suggests that these "cool" ions originated from the cold supersonic outflow, and that the destination ( $X$  distance) and/or the flux of this cold supersonic outflow to the tail plasma sheet significantly vary, although we have no clue to examine it.

Adding this velocity-filter effect, satellite that slowly traverses the inner magnetosphere can also detect the time-of-flight  
 320 effect of eastward drift because if the energy dependency of the drift velocity as mentioned in Section 4.1. This effect is seen in Figs. 7. After extracting temporal variation on the same L-shell using the differences between three spacecraft, and combining the observed electric field and average drift velocity, Yamauchi et al. (2006a) estimated the elapsed time as only 15-30 minutes (substorm onset was about 30 min before) after the start of dispersion with a start local time at around 6-8 MLT.

Thus, dispersion may start in the dawn sector instead of midnight sector as illustrated in Figs. 7h. This indicates that the  
 325 electric field in the midnight-dawn sector can be stronger than what was previously thought, particularly for severe substorms.



Such strong electric field is also suggested by high demarcation energy of  $> 40$  keV as mentioned above, and is theoretically possible when it is highly screwed.

#### 4.4 Dynamics of outflowing ions directly supplied from the ionosphere

As mentioned in Sections 3.2 and 3.3, some outflowing ions from ionosphere enters the inner magnetosphere directly inside the geosynchronous orbit, particularly in the nightside (Quinn and McIlwain, 1979; Hultqvist, 2002). Even "warm" ions  $< 100$  eV with nearly field-aligned pitch-angles are commonly found in the equatorial inner magnetosphere (Horwitz and Chappell, 1979; Yamauchi et al., 2013). These ions are not necessarily inside the loss-cone because energization to accelerate to suprathermal and hot energy involves perpendicular heating above the mirror point. They are normally without significant  $O^+$ . In this sense, this is similar to the cold supersonic flow or cold filling, and can be ignored in amount compared to plasmaspheric cold ions.

Fig. 8 shows one such example at 05:15-05:35 UT. The very weak dispersion (1 min from 30 eV to 200 eV) indicates short elapsed time ( $< 15$  min), although it is still longer than the travel time from the ionosphere ( $< 5$  min) for  $H^+$  outside the loss-cone. This means that source must be around 15 MLT and  $63^\circ$  Inv, which is lower latitude than where the beam-like outflow  $> 1$  keV is often observed (Lundin et al., 1995) but still within the region of outflow (Peterson et al., 2008). On the other hand,  $O^+$  case for such warm flow does exist. Fig. 7 shows an example.

The first wedge-like structure at around 23:45 UT in SC-1 and SC-4 has two part, low-energy  $O^+$  at  $< 300$  eV with peak at  $180^\circ$  pitch-angle and sub-keV trapped  $H^+$  afterward. These  $O^+$  appeared subsequently in SC1 (23:44-23:51 UT) and SC4 (23:50-23:55 UT) at nearly the same latitude (L value), without obvious energy-time dispersion (no time-of-flight effect), and thus limited to small source region, as illustrated in Figs. 7b. Considering the field-aligned velocity of low-energy  $O^+$  (20-40 km/s for 50-200 eV  $O^+$ ) and lack of mirrored ions outside the loss-cone, these  $O^+$  must have left the northern ionosphere at 8-9 MLT about 10-30 minutes continuously before the detection, and most likely no outflow before. This timing agrees with the substorm onset at around 23:10 UT, and with the elapsed time of eastward drifting ions that was calculated in 4.3. The late-morning to prenoon auroral and sub-auroral (closed geomagnetic field) region is known for strong ion outflow with high  $O^+/H^+$  ratio and significant enhancement with substorm activity (Øieroset et al., 2000; Peterson et al., 2008). This event shows how quickly outflow starts after the substorm onset with  $O^+$  dominance over  $H^+$ .

A similar field-aligned burst is also seen in Fig. 9 at 06:48:30 UT, first coming from southern hemisphere for  $< 100$  eV ions. The energy extends soon to nearly 1 keV with bouncing (nearly field-aligned bi-directional) signature. Unlike the  $E \times B$  drift 5 minutes before, these ions contain  $O^+$  (not shown here), indicating that they are directly coming from the ionosphere rather than a local heating. The ionospheric conjugate along the geomagnetic field corresponds to where the transpolar arc and the auroral bulge meets, according to the IMAGE FUV data (Fig. 9d). A detailed description should be reported in a separate paper. In addition, Fig. 9 shows a sudden change of pitch angles for keV ions at around 06:44 UT, without any signature in the sub-keV energy range. The timing and location corresponds to the westward travelling auroral bulge, and keV  $O^+$  flux was also enhanced although it is less clear than  $H^+$  signature (Yamauchi et al., 2009b). The energy and location indicates that these outflowing ions are accelerated by the parallel electric potential drop over the auroral bulge.



Once ions coming directly from the ionosphere start to drift, it is difficult to distinguish them from the magnetotail-origin  
360 low-energy ions just from energy spectrum. However, composition and particularly the pitch-angle distribution are often dif-  
ferent, as shown in Fig. 7 during active period. Fig. 8 shows another example. The repeated  $H^+$  bursts in from 05:07 UT to  
05:55 UT with low pitch angles show weak dispersion as time processes, whereas the simulated  $H^+$  wedge has a peak at nearly  
 $90^\circ$  pitch angle.

Such the mixing occurs even during quiet times and in large scale. Fig. 12 shows one such example (Giang et al., 2009).  
365 Wedge-like dispersed sub-keV  $H^+$  with low pitch angles during 00:55-01:18 UT is followed by the wedge-like dispersed  
sub-keV  $O^+$  with high pitch angles without  $H^+$  after 01:18 UT. Thus,  $H^+$  and  $O^+$  are anti-correlated with different pitch  
angles. Such anti-correlation is seen already from 00:20 UT. The wedge-like dispersion at low-energy indicates that these ions  
experienced eastward drift from the morning (or even from the midnight) sector, and the different pitch angles indicates that  
only  $O^+$  experienced substantial adiabatic energization and hence longer drift distance than  $H^+$ . Since both magnetic and  $E \times B$   
370 drifts are mass-independent, this observation suggests that  $H^+$  injection was closer to the Earth than  $O^+$  injection, and that  
such newer injection of  $H^+$  expelled the pre-existing  $O^+$ . The low-pitch angles for  $H^+$  also suggest that the injection point is  
in the inner magnetosphere rather than in tail plasma sheet.

The anti-correlation event is not often observed and all the events are observed during relatively quiet time with  $AE < 100$  nT  
(Giang et al., 2009). Some nearly correlated cases between  $H^+$  and  $He^+$  also show a small shift in terms of energy (or latitude),  
375 as shown in Fig. 13. The small shifts mean small differences of the start location of drift, and are expected from the difference  
of destinations of cold supersonic outflow with velocity filter effect. However, a majority of observations shows correlation  
between  $H^+$  and  $O^+$  in term of energy-latitude dispersion. These correlated cases indicate that the start location is the same  
between difference species, i.e., the same destination of outflowing ions in the plasma sheet without velocity filter effect.

This is reasonable for suprathermal and hot outflow because parallel velocity is similar between different species as men-  
380 tioned in Section 2.3, For cold ions, there is no direct observation of velocity ratio between different species. If the same  
energization mechanism involves for cold supersonic outflow and hot outflow, we expect even similar velocities and similar  
destination distances between different species.

#### 4.5 Local energization of low-energy ions

In previous subsections, three major sources of sub-keV ions in the inner magnetosphere are shown: (a) direct supply from the  
385 ionosphere including bouncing ones (e.g., Figs. 7-9), (b) drifting ions from the nightside plasma sheet (e.g., Fig. 11), and (c)  
local perpendicular heating of the plasmaspheric cold ions confined to the equator (e.g., Fig. 10). Almost all ion population in  
the inner magnetosphere observed by Cluster can be explained with these sources. However, mainly at around substorm onset,  
new ion population sometimes appears suggesting local energization.

##### 4.5.1 $He^+$ heating

390 While almost all the perpendicular heatings of plasmaspheric cold ions are locally confined to equator, we seldom observed  
local perpendicular heating of  $He^+$  without  $H^+$  signature away from equator. (Fig. 13) shows examples, with and without  $H^+$

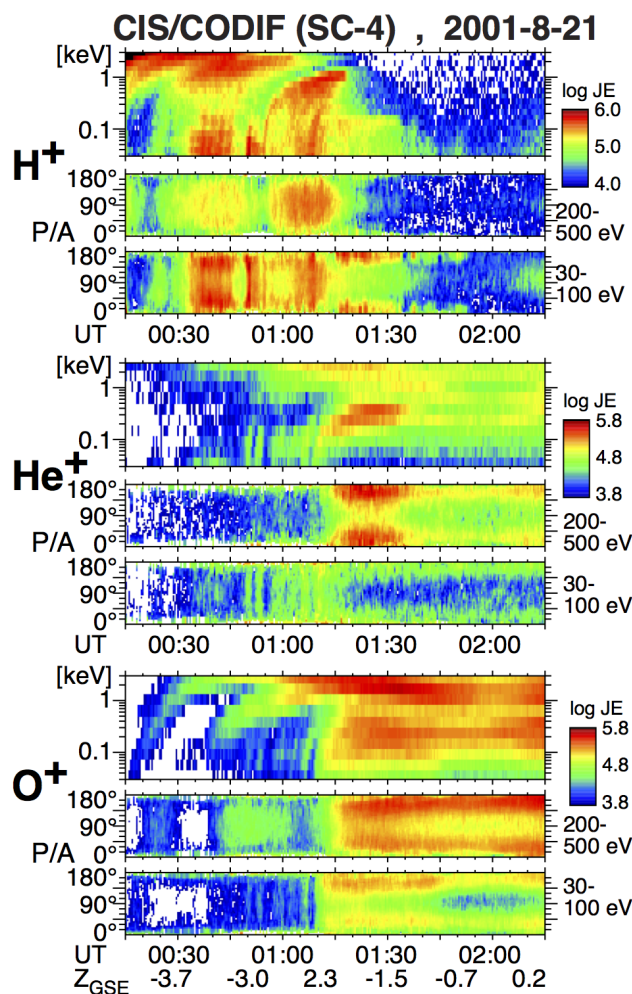


**Figure 12.** Cluster hot ion energy-time and energy-pitch angle spectrograms of differential energy fluxes ( $\text{keV cm}^{-2}\text{s}^{-1}\text{str}^{-1}\text{keV}^{-1}$ ) from spacecraft 4 on 21 August 2001 (Giang et al., 2009; Yamauchi et al., 2014a).

flow from the ionosphere (Yamauchi et al., 2014a). Local and occurrence frequency suggests that the wave mode related to this heating is different from the perpendicular heating near the equator. The absence of  $\text{H}^+$  strongly suggests a mass-dependent resonance frequency, although the associated wave mode has not been identified, like the equatorially trapped perpendicular heating (Fig. 10).

#### 4.5.2 PC-5 related energization

The associated wave mode can be ultra-low frequency (ULF), like Pc5 pulsation of  $10^{-2}$  Hz (Waite et al., 1986). (Fig. 14) shows one such example observed by Viking at around  $3 R_E$  (Yamauchi et al., 1996b). The trapped ions are bundled to certain energy together with the Pc5-range giant pulsation of azimuthal geomagnetic field in a synchronized manner. This ULF is also

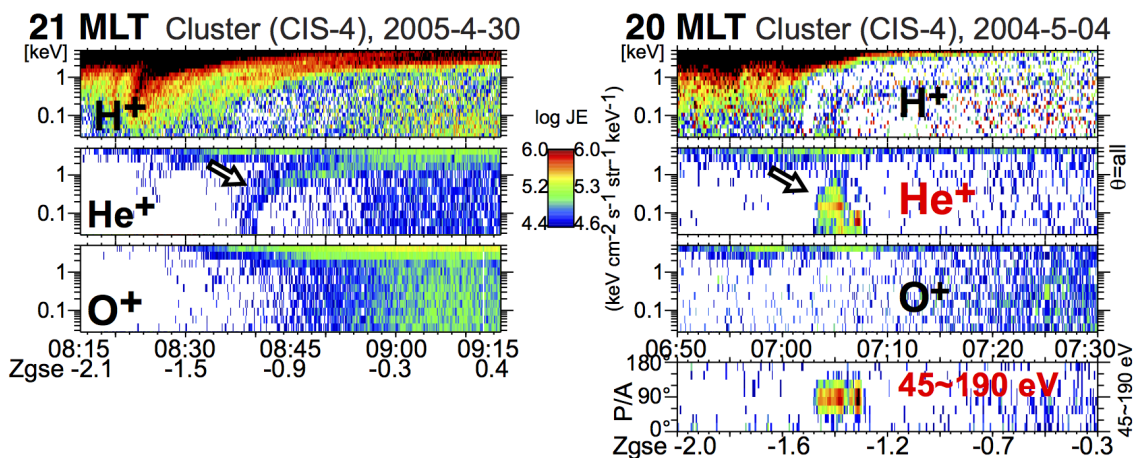


**Figure 13.** Cluster hot ion observation of  $\text{He}^+$  that shows different energy-time features from those of  $\text{H}^+$  and  $\text{O}^+$ . Unit of the differential energy fluxes (JE) is  $\text{keV cm}^{-2} \text{s}^{-1} \text{str}^{-1} \text{keV}^{-1}$ . (a) 30 April 2005 and (b) 4 May 2004 (Yamauchi et al., 2014a). For the second event, the energy-pitch angle spectrogram is also displayed.

400 detected at ground conjugate over several degrees. Such energy modulation synchronizing with ULF waves is often found at  $< 60^\circ$  Inv ( $L \leq 4$ , i.e., Cluster does not cover that region). In addition, conic-like energization near the loss-cone boundary was observed in this particular case. Unfortunately, this observation is unique over more than 700 Viking observations, and we do not have any good explanation of mechanism that caused the conic-like energization.

### 4.5.3 Energization by shock-like propagation

405 Local ion energization is not limited to local waves. Propagation of high-amplitude polarization electric field including shocks can also heat ions effectively. Although such finite-amplitude structures are very rare in the inner magnetosphere, they do exist for both propagating directions: sunward (Yamauchi et al., 2009b) and anti-sunward (Araki et al., 1997).

Fig. 15 shows an example of ion energization by the anti-sunward propagation of shock when interplanetary coronal mass ejection (ICME) with 2000 km/s velocity arrived the Earth at the beginning of the Halloween storm event on 29, October 2003 (Yamauchi et al., 2006b). The propagation velocity inside the inner magnetosphere was as fast as the ICME velocity without delay, and much faster than the propagation route through the ionosphere. In addition, spacecraft in the midnight sector near the equatorial plane detected a dipolarization of geomagnetic field started only 20 sec after the arrival of this shock at midnight, indicating that this triggered the dipolarization. Note that this is rather a unique event and this onset mechanism may not be generalized.

415 The opposite example, i.e., sunward propagation of large-amplitude polarization electric field is also found in the equatorial inner magnetosphere at around  $L=4$  after the substorm onset on 19, May 2002 (Yamauchi et al., 2009b). Fig. 9 shows the overview and summary illustrations. At around 06:43 UT, Cluster detected plasmaspheric cold  $\text{H}^+$  and  $\text{He}^+$  drifting duskward (perpendicular to the magnetic field) with high velocity up to 50-60 km/s Electric field measurement shows anti-sunward DC

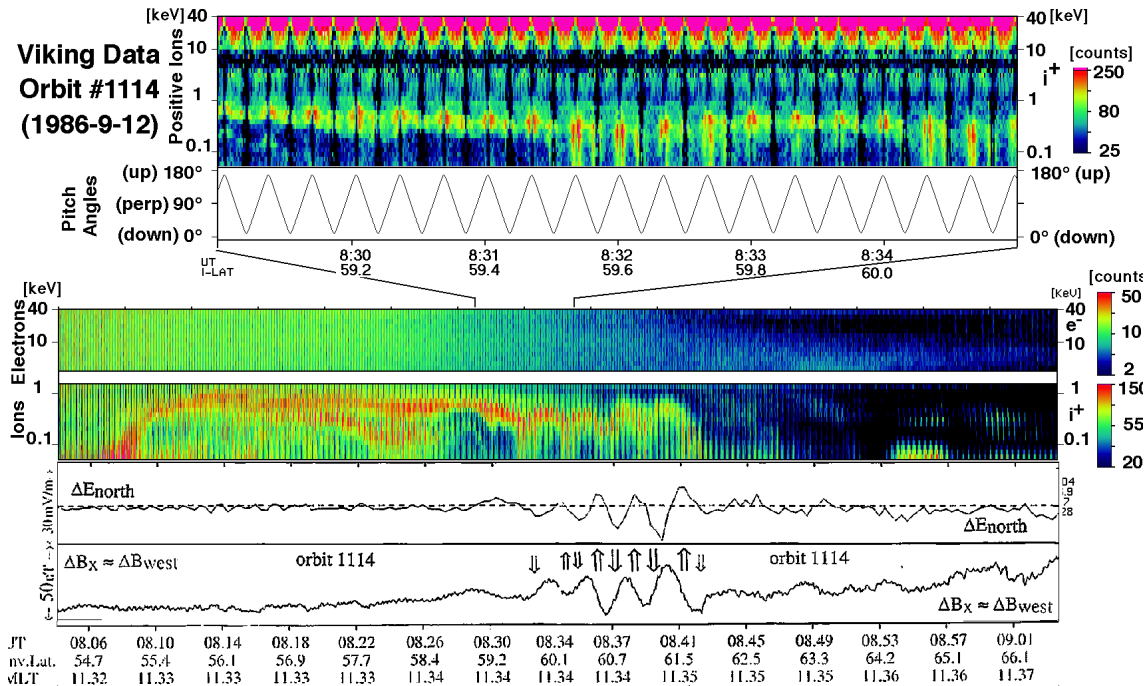


**Figure 14.** Viking data over the dayside subauroral region during a giant pulsation after large substorm on 12 September 1986 (Yamauchi et al., 1996b). Energy-time spectrograms of ions and electron, electric field, and one magnetic field component (the other components are almost constant) are displayed. The empty arrows in the magnetic field are the direction of the field-aligned current in case the variation includes some spatial structure. The spacecraft was in conjugate with Finish geomagnetic chain during the giant pulsation.

field up to 10 m/V, in agreement with the  $E \times B$  drift velocity for the observed geomagnetic field. Relative timing between  
 420 four Cluster spacecraft indicated that this finite-amplitude E-field propagated sunward with velocity of 5-10 km/s, and hence  
 the electric field is the polarization field with positive charges leading on the front side as illustrated in Figs. 9e and 9f. In the  
 ionosphere, this electric field is mapped to the substorm auroral bulge at 19 MLT that has exactly the same sunward propagation  
 velocity as this polarization electric field in the equatorial magnetosphere.

One unique feature is that the ring current ions at energy rangy 70-1000 keV showed a mass-dependent flux enhancement  
 425 together with mass-dependent decrease of ions at energies above and below. The energy ratio of enhancing  $O^+$ ,  $He^+$  and  $H^+$   
 are about 16:4:1.5, i.e., all species have nearly the same gyration speed of about 3000 km/s. The mass-dependent decrease  
 of flux at higher energy also has the similar gyration velocity for all species (about 5000 km/s), whereas the decrease of  
 flux at lower energy (Fig. 9c) was seen only in heavy ions at high pitch angles but not  $H^+$  (not shown here), for which the  
 corresponding energy is outside the lower energy threshold of the ring current. Since both the magnetic and  $E \times B$  drifts are  
 430 mass-independent, the energy enhancement is less likely caused by drifting of new injections from the nightside. Therefore,  
 the propagating polarization structure with large amplitude most likely caused the mass-dependent flux enhancement of ions.

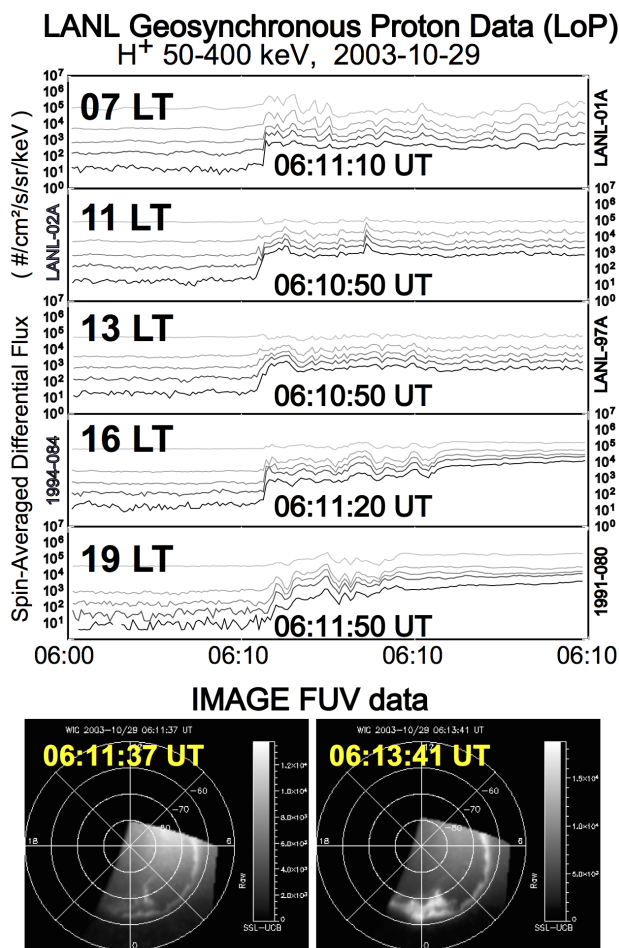


**Figure 15.** Top: Energetic proton flux (50-400 keV) observed by the LANL geosynchronous satellites (LANL-01A at 07 LT, LANL-02A at 11 LT, LANL-97A at 13 LT, 1994-084 at 16 LT, and 1991-080 at 19 LT) during the initial phase of the 2003-10-29 storm (06:00-06:30 UT). Bottom: IMAGE FUV data that shows quick expansion of auroral substorm at around 06:12 UT, which is confirmed by ground geomagnetic field data (Yamauchi et al., 2006b).

One possibility is that ions with gyrating velocity higher and lower than 3000 km/s are somewhat decelerated/accelerated by this structure, but the mechanism is unknown.

#### 4.6 Composition

435 Since the composition of inner magnetospheric ions ( $H^+/He^{2+}/He^+/O^+/N^+$  ratio) is different for different source or energization mechanism, it is quite different at different location (e.g., local time) in the inner magnetosphere (Wellings et al., 2011). Even for the same source such as the tail plasma sheet, local time dependence can occur because, for example, bursty  $O^+$  return flow is not aligned to bursty  $H^+$  return flow (Nilsson et al., 2016). Such statistics together with the mass-dependent



energization in the inner magnetosphere as listed above remains as unsolved issues. On the other hand, general abundance  
440 of heavy ions (both  $O^+/H^+$  ratio and  $N^+/O^+$  ratio) is known to increase with geomagnetic activity (Hamilton et al., 1988;  
Daglis et al., 1999; Maggiolo and Kistler, 2014), as is expected from the higher outflow rate from the ionosphere for higher  
geomagnetic activities as described in Section 2.3. Note that this does not mean less geomagnetic dependence on the escaping  
 $O^+$  to the space because the  $O^+$  outflow into the largest escape route in the cusp, plasma mantle, and magnetosheath shows  
nearly power law dependence to the solar wind energy input and geomagnetic disturbance, i.e., exponential increase with  $K_p$   
445 (Slapak et al., 2017a, Schillings et al., 2019).

#### 4.7 Loss process

Among the primary motion by the ion drifts, all drift components except the  $E \times B$  drift by the external electric field keep ions  
trapping in the inner magnetosphere, like the inner radiation belt where the effect of the external electric field is negligible.  
However, the  $E \times B$  drift by the external electric field drives inner magnetospheric ions in one direction rather than rounding the  
450 Earth, making them to reach the magnetopause. Once the ions reach the magnetopause, these drifting ions can leak outside the  
magnetopause without reconnection (Sibeck et al., 1987; 1999; Marcucci et al., 2004) and start moving in the same direction  
as the anti-sunward (e.g., magnetosheath) flow through the ion pickup process. This is called the magnetopause shadowing and  
is the most effective to ions with high pitch angle (cf.  $\alpha = 90^\circ$  in Equation 1) for the same energy (Blanc et al., 1999), making  
ion pitch-angle distribution at equator oblique ("butterfly" distribution).

455 The magnetopause shadowing is well known for the detached cold plasmaspheric plumes as described in Section 4.2. Even  
the hot sub-keV ions in the dayside inner magnetosphere may experience the same evacuation mechanism from the inner  
magnetosphere because the westward magnetic drift cancels the east corotation to stay in the same local time sector for  
sufficiently a long time to reach the magnetopause by the remaining sunward convection component. This means that, if no  
ions are supplied from the nightside plasma sheet, sub-keV (and even keV) ions will be evacuated through the magnetopause  
460 shadowing. Such ion evacuations are observed at the start of magnetic storm before the first ions inject (Hultqvist et al., 1981,  
Yamauchi and Lundin, 2006). Even a substantial portion of tens keV ions are most likely lost through the magnetopause  
shadowing because this is the only available explanation to make "butterfly" pitch-angle distribution.

For high-energy ions, the magnetopause shadowing becomes less important compared to the other loss mechanisms such as  
the charge exchange, Coulomb collisions with thermal plasma, and pitch-angle scattering to the loss cone by waves (Blanc et  
465 al., 1999; Ebihara and Ejiri 2003). Efficiency of these local processes of ion loss is well understood for energy  $> 1$  keV (Fox et  
al., 1991; Ebihara and Ejiri 2003), with minimum lifetime for ordinary ring current energy range (around 10 keV for  $H^+$  and  
 $> 100$  keV for  $O^+$ ). Here, Coulomb collision mainly decreases the energy rather than scattering into the loss cone, and hence  
less contributing to the ion loss from the inner magnetosphere than its lifetime (Fox et al., 1991). Ion drift simulations using  
these efficiencies has been successful, supporting the charge exchange as the dominant loss mechanism for the ordinary ring  
470 current ions than the scattering into the loss cone for radiation belt particles (Blanc et al., 1999; Ebihara and Ejiri 2003).

On the other hand, the efficiency for sub-keV ions becomes relatively small comparing to the time scale of the magnetopause  
shadowing. In fact, ion drift simulations with charge-exchange loss alone can reproduce the energy-latitude dispersion of sub-



keV ions in the dayside (Ebihara et al., 2001, 2004; Yamauchi et al., 2009a, 2014b). The superposed statistics sorted in terms of the delay-time from the substorm onset (injection of the sub-keV ions) also showed a sudden decrease of the observation rate of "substorm fossil" ions when these ions reaches the noon sector (Yamauchi and Lundin, 2006). Since the local loss mechanism is nearly constant in time whereas the magnetopause shadowing is the most efficient in the noon sector for sub-keV ions, the magnetopause shadowing is the most effective loss mechanism followed by the charge-exchange mechanism.

Among these loss mechanisms, magnetopause shadowing contributes the complete loss of ions from the magnetosphere whereas the scattering into the loss cone brings ions back to the ionosphere. Charge exchange is in between when only trapped ions bouncing in the magnetic bottle are considered, because the energetic neutral atoms (ENA) produced by this mechanism may point both toward the Earth and toward the space depending on the motion of the source ions. Since the neutral atmospheric density is maximum near the mirror point where the ions are gyrating in nearly horizontal directions, roughly half the ions move toward the Earth and half toward the space. This applies even to bouncing ions with low pitch angles because loss cone at equator is order of only  $1^\circ$ . Altogether, approximately half the ENA is lost and half retuning to the atmosphere.

## 5 Consequences of $O^+$ escape to space

### 5.1 Summary of $O^+$ budget

Fig. 5 summarizes the major ion escape routes that are described in this paper. First route (marked as (d) in Fig. 5) is the direct mixing with the solar wind into the magnetosheath and plasma mantle. Since hot  $O^+$  observed in that region have been energized into the hot ion energy range of Cluster ( $> 28$  eV), contributions from  $O^+$  with less energy must be very minor. All hot  $O^+$  in the magnetosheath and large part of  $O^+$  in the plasma mantle contributes to the net escape. Slapak et al. (2013, 2017a) and Schilling et al. (2019) have estimated the  $O^+$  loss rate after considering the destinations of the plasma mantle flow.

The second route (marked as (c) in Fig. 5) is through the tail lobe and the tail plasma sheet, from where some ions further move anti-sunward and some return Earthward. For hot  $O^+$ , Slapak et al. (2017b) and Slapak and Nilsson (2018) estimated for both anti-sunward flux and sunward flux in both plasma sheet and tail lobe. For cold supersonic ion, Engwall et al (2009) estimated total amount of ions flowing lobe into the tail plasma sheet as  $8 \times 10^{25} \text{ s}^{-1}$ . Considering very low  $O^+/H^+$  ratio ( $< 10^{-2}$ ), this means that total  $O^+$  flux in the lobe is less than  $0.1 \times 10^{25} \text{ s}^{-1}$ , and can be ignored compared to the first route when considering the  $O^+$ .

The retuning flow is not necessarily returns to the ionosphere. Rather, a large portion (more than half for the sub-keV ions and near half for for the ring current ions) escape through the magnetopause shadowing and the charge exchange. The same loss mechanisms to the space applies to ions coming from nightside auroral zone such as through boundary plasma sheet (BPS), a region with structured ions and electrons around keV (Winningham et al., 1975; Woch and Lundin, 1993). Although the nightside outflow region lies inside the closed field line region, majority of the outflowing  $O^+$  is not precipitating into the other hemisphere as mentioned in Sector 3.3, and can be included as the plasma sheet ions.



The third route (marked as (b) in Fig. 5) is the direct supply to the inner magnetosphere such as Fig. 7. While there are some  
505 statistics using geosynchronous satellite, so far no statistics exists for  $O^+$  flux. On the other hand, the flux, particularly for  $O^+$ ,  
is very small, and can safely be ignored when discussing the total amount of escape.

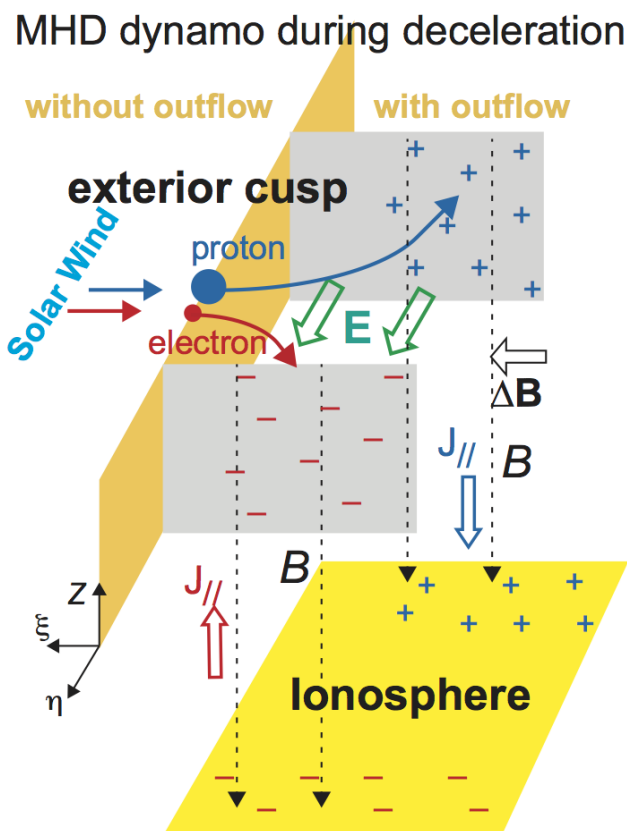
The last route is through refilling the plasmasphere (marked as (a) in Fig. 5). Although dominated by  $H^+$  (90%) and  $He^+$   
(10%) with only 1-5% for  $O^+$  (Sandel, 2011), the escaping amount is massive for both sporadic plume (peak  $10^{27} s^{-1}$  with  
about 5-10% of time) and continuous plasmaspheric outward wind up to  $5^{26} s^{-1}$  (Sandel and Denton, 2007; Darrouzet et al.,  
510 2008; Dandouras et al., 2013). Therefore, average  $O^+$  escape rate can be as much as  $0.3 \times 10^{25} s^{-1}$  for plume and  $1.5 \times 10^{25} s^{-1}$   
for outward wind. Because of its low energy with very small field-aligned velocity, majority of them are expected to escape by  
the magnetopause shadowing or tailward detachment.

Table 1 summarizes the  $O^+$  escape rate from the present Earth through these major escape routes. The direct escape from  
the magnetosheath and plasma mantle accounts for the majority of  $O^+$  escape from the present Earth. This also means that  
515 the non-thermal heating is the major escape mechanism among various escape mechanisms. The total escaping flux through  
this route drastically increases with the geomagnetic activities and with the solar wind energy input, as summarized in Table 1  
and Fig. 3 (Slapak et al., 2017a; Schillings et al. 2017, 2019). Since  $K_p$  is defined as nearly logarithmic scale of geomagnetic  
disturbances in nT, the exponential dependence given in Table 1 means nearly power law dependence to the geomagnetic  
disturbance. The power law dependence is also seen between the solar wind energy input and the escape flux (Schillings et al.,  
520 2019). The consequence of such large amount of  $O^+$  escape is wide. For example, importance of  $O^+$  in the magnetospheric  
dynamics such as the substorm onset has long been discussed and studied (Kistler et al., 2005; Kronberg et al., 2014). Here  
two substances that have been underestimated until recent are briefly explained.

## 5.2 Importance of $O^+$ escape on solar wind interaction

The active roles of the mixing of  $O^+$  into the solar wind have long been overlooked, although its importance has been sug-  
525 gested for long (Yamauchi and Lundin, 1997; Winglee et al., 2002). This is partly because the  $O^+$  density is considered small  
compared to the incoming solar wind density before Cluster made quantitative statistics of the  $O^+$  abundance in the incoming  
solar wind in the magnetosheath, the cusp, and the plasma mantle.

The observed  $O^+$  abundance in the plasma mantle is about 1% observed and hence nearly 20% of mass density due the 16-  
times heavier mass of  $O^+$  than  $H^+$ . When the mass-loading of  $O^+$  is completed, i.e., anti-sunward velocity of  $O^+$  catch up that  
530 of solar wind, the 20% mass density ratio of  $O^+$  means a 10% decrease of the solar wind velocity ( $u_{sw}$ ) and a 10 % decrease  
of total kinetic energy ( $K$ ) of the solar wind and the mass-loading  $O^+$  (Yamauchi and Slapak, 2018a). Cluster observation  
of anti-sunward velocities of  $O^+$  (increasing toward tail) and  $H^+$  (decreasing toward tail) support the mass loading process  
(Yamauchi and Slapak, 2018b). Unlike comets and unmagnetized planets, the initial charge separation during the deceleration  
of the solar wind by the mass loading can flow along the geomagnetic field to the conducting ionosphere to cancel the charge,  
535 as illustrated in Fig. 16. Thus, the surplus kinetic energy can maintain the electric current circuit that closes near the ionospheric  
cusp that is the mapping region of the entire the mass-loading area.



**Figure 16.** Illustration of the azimuthal charge separation when the solar wind inflow is decelerated by the start of mass loading with the outflowing ionospheric ions (Yamauchi and Slapak, 2018b). The boundary of the start of the outflowing region is shown with orange plane. The positive (negative) charges are always deflected by the geomagnetic field  $B$  in the opposite directions to (along) the motional electric field  $E$ , resulting in a dynamo current that causes a magnetic deviation ( $\Delta B$ ). Because of the connectivity to the ionosphere where the charges can move across the magnetic field, the accumulated charges form a current circuit through the field-aligned currents ( $J_{//}$  with blue and red arrows giving directions along  $B$ ) closing in the ionosphere.

The principle is the same as the reconnection (Dungey, 1961; Axford and Hines, 1961) except that this process works only where  $O^+$  can access the solar wind rather than the geomagnetic open/closed configuration, and hence this mechanism works only local region rather than globally. Thus, the current system by the mass-loading is independent from the global current system, and can explain the observed independency between the cusp region 1 field-aligned current and non-cusp dayside region 1 field-aligned current (Ohtani et al., 1995; Yamauchi and Slapak, 2018a). The concept of such "second openness" is originally proposed by Vasyliunas (1995), where the open-closed boundary are defined twice, first by the solar wind access point to the magnetosphere, and second by the ionospheric ion access point to the solar wind.

540



Yamauchi and Slapak (2018b) obtained upper limit of the energy extraction rate by the mass loading of escaping ions ( $\Delta K$ )  
545 as

$$\Delta K \sim -\frac{1}{4} F'_O u_{sw}^2 \quad (4)$$

where  $F'_O$  is total mass flux of the escaping ions into the mixing region with the solar wind (the cusp, the plasma mantle,  
and the magnetosheath). Although the process is local, the energy conversion rate of 10% (cf. the same order of magnitude  
as the reconnection rate) gives about  $\Delta K \sim 3 - 10 \times 10^9$  W, which is sufficient to explain the cusp current system (Potemra,  
550 1994, Yamauchi and Slapak, 2018a). Cluster data also showed a substantial deceleration of the solar wind together with the  
anti-sunward acceleration of  $O^+$  in the plasma mantle (Yamauchi and Slapak, 2018b).

Eq. 4 does not include the solar wind density or IMF in the first approximation. Instead,  $\Delta K$  depends on the total escaping  
mass flux mixing with the solar wind ( $F'_O$ ), which increases for high solar wind energy input (Schillings et al., 2019). Since the  
total escaping flux strongly depends on both Kp and the solar wind dynamic pressure (Fig. 3), particularly on velocity when the  
555 upstream solar wind velocity exceeds 500 km/s (Slapak et al., 2017a; Schillings et al., 2019), this current system forms a strong  
positive feedback between the escaping flux and the extracting energy, guaranteeing higher energy conversion and escape rate  
for faster solar wind. This agrees with more drastic response of dayside outflow to Kp compared to the nightside outflow. In  
this sense, the  $O^+$  outflow is relevant even to the space weather in addition to the ionospheric physics (Yamauchi et al., 2018).

### 5.3 $O^+$ escape on geological scale

560 Before Cluster confirmed the large amount of  $O^+$  escape through the direct mixing with the solar wind,  $O^+$  escape has  
been considered negligible in the evolution of the atmospheric and biosphere even in geological scale over > 1 billion years  
( $\sim 3 \times 10^{16}$  s). If one uses simple values of  $10^{26} \text{ s}^{-1}$  ( $\sim 0.3 \text{ kg/s}$ ), total amount of oxygen loss to the space over 1 billion years  
is only  $\sim 1 \times 10^{16} \text{ kg}$  and is small compared to the present atmospheric mass ( $1 \times 10^{18} \text{ kg}$  for oxygen and  $4 \times 10^{18} \text{ kg}$  for  
nitrogen).

565 However, the solar EUV, solar rotation, and solar wind in the ancient time are most likely much higher and faster than  
the present days due to much faster rotation compared to the present days (Ribas et al., 2005; Wood, 2006; Airapetian and  
Usmanov, 2016). The fast rotation also means strong solar dynamo magnetic field and IRF in the ancient time. Due to the  
exponential dependence of the  $O^+$  escape on Kp as summarized in Table 1, the ancient condition means very high escape rate  
exceeding  $10^{27} \text{ s}^{-1}$ . This gives already  $> 10^{17} \text{ kg}$  or 10% of atmospheric oxygen content over 1 billion years. Considering that  
570 the biological activity is sensitive to O/N ratio of the atmosphere (e.g., Loesche, 1969; Hill, 1976; Harrison, 2010), this can no  
longer be ignored. If the escape rate reaches  $10^{28} \text{ s}^{-1}$ , as is suggested by Krauss et al. (2012) and Slapak et al. (2017a), only  
100 million years is enough to affect the bioactivity.

Thus, although the oxygen can be supplied from the ocean, the atmospheric escape to the space could have played some  
role in the evolution of the biosphere. However, before any quantitative estimate of modelling, we must also consider many  
575 other factors such as the neutral escape due to the higher UV flux and weaker terrestrial dynamo (smaller magnetosphere) in  
the ancient time, as illustrated in Fig. 17 (Yamauchi and Wahlund, 2007). High UV increases the thermospheric temperature,

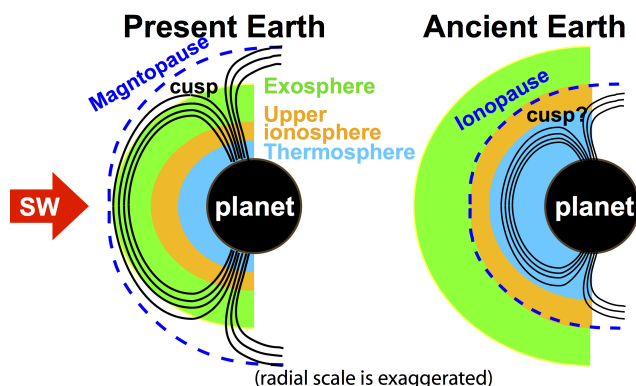


**Figure 17.** Illustration of differences in the magnetosphere, exosphere, and ionosphere between the present and ancient Earth (cf. Yamauchi and Wahlund, 2007).

**Table 2.** Escape energy from the Earth at different height

height	500 km	2000 km	10000 km
velocity	10.8 km/s	9.8 km/s	7.0 km/s
O	9.7 eV	8.0 eV	4.1 eV* <sup>1</sup>
N	8.5 eV	7.0 eV	3.6 eV* <sup>2</sup>

\*1:  $O_2^+ + e^- \rightarrow 2O + 1.7 \text{ eV}$

\*2:  $N_2^+ + e^- \rightarrow 2N + 3.6 \text{ eV}$

and hence expands the thermosphere and the exosphere, although cooling by a larger amount of CO<sub>2</sub> in the ancient atmosphere will somewhat ease this change (Tian et al., 2008). The increased exobase altitude reduces the escape energy as summarized in Table 2, and makes thermal escape after photochemical heating much more effective.

580 The weaker terrestrial dynamo and stronger solar wind in the ancient time set back the sub-solar distance of the magnetopause where the solar wind dynamic pressure and the magnetic pressure of the geomagnetic field balances (Yamauchi and Wahlund). As the result, neutrals of the expanded exosphere are exposed to the solar wind with significant amount like the Martian case (Yamauchi et al., 2015). The expanded thermosphere and exobase are normally accompanied by an expanded ionosphere, making the Earth even more non-magnetized type planet in terms of the atmospheric escape. Altogether, neutral  
 585 escape might become important as summarized in Table 3, for many of which we do not have enough observational knowledge for quantitative modelling. Nevertheless we at least expect that the escape rate should be more than what is obtained only from the ion escape. In other words, less than 100 million years might be enough for atmospheric escape to affect the bioactivity in the past in the geological scale.

Our observational knowledge is not sufficient for even the present-day's neutral distribution in the exosphere and upper  
 590 thermosphere. The empirical average such as the MSIS model is not sufficient to model the upper thermosphere and exosphere



**Table 3.** Major mechanism of atmospheric loss to the space

mechanism	present Earth	ancient Earth	knowledge needed
Jeans escape	(negligible)	yes?	present exosphere
Hydrodynamic blow off	(negligible)	yes?	present exosphere
Momentum exchange	(negligible)	yes?	present exosphere
Photochemical energization	(negligible)	yes	present exobase
Charge-exchange	yes	?	ring current
Atmospheric sputtering	(negligible)	yes?	past cusp
Ion pickup	(negligible)	yes	
Ions accelerated by EM field reach SW	yes	yes	
Large-scale momentum transfer and instabilities by the solar wind interactions	yes	yes?	past magnetosphere
Magnetopause shadowing (ions)	yes	yes?	past ring current
Plasmaspheric wind and plumes	yes	yes?	past plasmasphere

when modelling the escape (e.g., Meier et al., 2015; Lakhina and Tsurutani, 2017). For example, local extent of the exosphere, which is one of the most basic parameter, is sensitive to solar UV and geomagnetic activities (Zoennchen et al., 2015, 2017), but the data is not sufficient to include them in the empirical model. The extent of the exosphere that is estimated from the production of newly ionized exospheric hydrogen changes by order of magnitude (seen as pickup ion flux) with only factor of 2 difference in the solar UV (Yamauchi et al., 2015). However, similar in-situ study at the Earth is not possible due to the lack of proper neutral instruments at altitude 500-5000 km range. To answer neutral dynamics and its escape from altitude above the exobase, we need a dedicated space mission to study both ion escape and neutral escape from the present Earth (Dandouras et al., 2016, 2018).

## 6 Discussion

In this paper, the transport of the terrestrial ions and the behaviors of hot heavy ions in the inner magnetosphere, where outflowing ions from different routes convolute, have been reviewed, with stress on those overlooked before the Cluster age. Cluster is the first mission that covers all important region for ion escape including polar magnetospheric boundary and plasmasphere with instruments that allows quantitative estimate, as summarized in Table 1. To cover the most important route and dynamics that is relevant to  $O^+$  escape, many ion phenomena are skipped. A full description requires an entire book.

The major loss mechanisms of the inner magnetospheric ions, if the change in energy is ignored, are magnetopause shadowing, the charge exchange, and the scattering to the loss cone. Because of energy dependence of these mechanisms, return rate of  $O^+$  to the ionosphere is higher for higher energy ions, but its upper limit is about 50%. In other words, the energization in the inner magnetosphere increases the return rate, but by not more than a factor of two. This is in contrast to the energization



610 above the ionosphere, which enhances the escape rate. Since the  $O^+$  return rate entering the inner magnetosphere is about 50% or less, while all the other outflowing ions escape to the space, the most important factor that determines the ion escape is the total outflow flux above the ionosphere. In this sense, the outflow value at 2000-4000 km altitude is the most important but only if the ion instrument can covers all the energy range.

The consequences of the  $O^+$  outflow and dynamics have wide aspects including the ionospheric physic, solar wind interaction with the magnetosphere, space weather, and the astrobiology, in addition to the effect on the magnetospheric activities such as substorms (e.g., Kistler et al., 2005; Kronberg et al., 2014). For example, the outflow flux is sufficient to activate the mass-loading type energy conversion from the solar wind to the electric current system that closes in the cusp ionosphere, which is independent from the current system driven by the global solar wind-magnetosphere interaction (Yamauchi et al., 2018b). The total escape rate of  $O^+$  to the space might have even played some role on the evolution of the biosphere through the change in the atmospheric composition of more than few percent (Slapak et al., 2017a; Dandouras et al., 2018). However, 620 these new applications are not yet quantitatively confirmed by dedicated observations or modellings, with only preliminary indirect observations or models (Winglee et al., 2002; Yamauchi et al., 2018b). Dedicated works and missions are needed to answer all these indications.

## 7 Conclusions

The ion outflow from the ionosphere can be classified into three categories when observing in the magnetosphere: (1) cold filling, (2) cold supersonic outflow, and (3) suprathermal and hot outflow. The outflowing suprathermal ions ( $< 50$  eV) above the ionosphere are most likely observed as hot ions in the magnetosphere. Direct destinations of these outflow (Fig. 5) ranges from the plasmasphere (innermost) to direct entry into the solar wind in the polar region (outermost). From these destinations, ions start to either circulate in the magnetosphere or escape to the space. Out of these three type of outflow, hot outflow alone causes high escape rate to the space for  $O^+$  as summarized in Table 1, making the non-thermal heating as the major escape 630 mechanism among various escape mechanisms (Table 3).

As the result of the secondary transport (circulation) and direct injection, the inner magnetosphere becomes a zoo of many different ions and different mechanisms of energization and transport. Some of these mechanisms, particularly for low energy ions, are still un-understood. Particularly, Cluster observed many mass-dependent energization and transport (e.g., Figs. 9a, 10, 12, and 13), although the observations are made inside the geosynchronous distance where the mass-independent drift theory 635 is well qualified.

The obtained total flux of terrestrial ion escape and its drastic dependency to the solar wind condition indicates that the ion outflow plays active roles on two subjects that have been overlooked in the past, in addition to role in the magnetospheric dynamics. One is the mass-loading effect into the solar wind, which can explain the energy conversion to sustain the cusp current system in the order of magnitude. This interaction promotes the second openness of the magnetosphere, where the open-closed boundary are defined twice, first by the solar wind access point to the magnetosphere, and second by the ionospheric ion access point to the solar wind. The other is the influence on the atmospheric evolution in the geological scale after taking 640



into account of the higher solar and solar wind activity in the past, although more complete observations and modelling are needed to answer this question. Such study requires a new dedicated mission on atmospheric escape.

645 *Data availability.* Cluster data data is available at Cluster Science Archive through [www.cosmos.esa.int/web/csa/access](http://www.cosmos.esa.int/web/csa/access)

*Code and data availability.* Cluster plotting software is available at Cluster Science Archive

*Competing interests.* No competing interest exists

650 *Acknowledgements.* The author appreciates EGU in offering special opportunity to make lecture at general assembly 2019. The author thanks R. Lundin, I. Dandouras, Y. Ebihara, H. Nilsson, and all past co-authors of authors work in preparing the manuscript and the EGU lecture. The author would like to dedicate this work as memory for Prof. Emer. Bengt Hultqvist, the first director of Swedish Institute of Space Physics, who passed away February 2019.



## References

- 655 Daglis, I. A., Thorne, R. M., Baumjohann, W., and Orsini, S.: The terrestrial ring current: Origin, formation, and decay, *Rev. Geophys.*, 37, 407-438, doi:10.1029/1999RG900009, 1999.
- Alfvén, H., and Fälthammar, C.G.: *Cosmical Electrodynamics, Fundamental Principles*, Clarendon, Oxford, 1963.
- Airapetian, V.S., and Usmanov, A.: Reconstructing the Solar Wind from Its Early History to Current Epoch, *Astrophys. J. Lett.*, 817, L24, doi:10.3847/2041-8205/817/2/L24, 2016.
- 660 André, M.: Previously hidden low-energy ions: a better map of near-Earth space and the terrestrial mass balance, *Phys. Scr.*, 90, 128005, doi:10.1088/0031-8949/90/12/128005, 2015.
- Araki, T., Fujitani S., Emoto M., Yumoto K., Shiokawa K., Ichinose T., Luehr H., Orr D., et al.: Anomalous sudden commencement on March 24, 1991, *J. Geophys. Res.*, 102, 14075-14086, doi:10.1029/96JA03637, 1997.
- Arvelius, S., Yamauchi, M., H. Nilsson, R. Lundin, Y. Hobara, H. Reme, M.B. Bavassano-Cattaneo, G. Paschmann, A. Korth, L.M. Kistler, and G.K. Parks (2005), Statistics of high-altitude and high-latitude O<sup>+</sup> ion outflows observed by Cluster/CIS, *Ann. Geophys.*, 23, 1909-1916, doi:10.5194/angeo-23-1909-2005, 2005.
- 665 Axford, W.I., and Hines, C.O., (1961), A unifying theory of high-latitude geophysical phenomena and geomagnetic storms, *Can. J. Phys.*, 39: 1433-1464, doi:10.1139/p61-172, 1961.
- Blanc, M., Horwitz, J.L., Blake, J.B., Daglis, I., Lemaire, J.F., Moldwin, M.B., Orsini, S., Thorne, R.M., and Wolfe, R.A.: Source and loss processes in the inner magnetosphere, Chapter 4 in *Magnetospheric Plasma Sources and Losses*, edited by B.Hultqvist et al., Kluwer academic publication, *Space Sci. Rev.*, 88, 137-206, doi:10.1023/A:1005203817354, 1999.
- 670 Cattell, C., Johnson, L., Bergmann, R., Klumpar, D., Carlson, C., McFadden, J., Strangeway, R., Ergun, R., Sigsbee, K., and Pfaff, R.: FAST observations of discrete electrostatic waves in association with down-going ion beams in the auroral zone, *J. Geophys. Res.*, 107, 1238, doi:10.1029/2001JA000254, 2002.
- 675 Chappell, C. R.: Recent satellite measurements of the morphology and dynamics of the plasmasphere, *Rev. Geophys.*, 10, 951-979, doi:10.1029/RG010i004p00951, 1972.
- Chappell, C.R., Olsen, R.C., Green, J.L., Johnson, J.F.E., and Waite, J.H.Jr: The discovery of nitrogen ions in the Earth's magnetosphere, *Geophys. Res. Lett.*, 9, 937-940, doi:10.1029/GL009i009p00937, 1982.
- Chappell, C. R., Moore, T. E., and Waite, J. H.: The ionosphere as a fully adequate source of plasma for the Earth's magnetosphere, *J. Geophys. Res.*, 92, 5896-5910, doi:10.1029/JA092iA06p05896, 1987.
- 680 Chappell, C.R., Huddleston, M.M., Moore, T.E., Giles, B.L., Delcourt, D.C.: Observations of the warm plasma cloak and an explanation of its formation in the magnetosphere, *J. Geophys. Res.*, doi:10.1029/2007JA012945, 2008.
- Collin, H. L., Quinn, J. M., and Cladis, J. B.: An empirical static model of low energy ring current ions, *Geophys. Res. Lett.*, 20, 141-144, doi:10.1029/93GL00066, 1993.
- 685 Craven, P. D., Olsen, R. C., Chappell, C. R., and Kakani, L.: Observations of molecular ions in the Earth's magnetosphere, *J. Geophys. Res.*, 90, 7599-7605, doi:10.1029/JA090iA08p07599, 1985.
- Craven, P. D., Gallagher, D. L., and Comfort, R. H.: Relative concentration of He<sup>+</sup> in the inner magnetosphere as observed by the DE 1 retarding ion mass spectrometer, *J. Geophys. Res.*, 102, 2279-2289, doi:10.1029/96JA02176, 1997.



- Cully, C. M., Donovan, E. F., Yau, A. W., and Arkos, G. G.: Akebono/Suprathermal Mass Spectrometer observations of  
690 low- energy ion outflow: Dependence on magnetic activity and solar wind conditions, *J. Geophys. Res.*, 108(A2), 1093,  
<https://doi.org/10.1029/2001JA009200>, 2003.
- Daglis, I. A., Thorne, R. M., Baumjohann, W., and Orsini, S. (1999), The terrestrial ring current: Origin, formation, and decay, *Rev. Geophys.*,  
37, 407-438, doi:10.1029/1999RG900009
- Dandouras, I.: Detection of a plasmaspheric wind in the Earth's magnetosphere by the Cluster spacecraft, *Ann. Geophys.*, 31, 1143-1153,  
695 doi:10.5194/angeo-31-1143-2013, 2013.
- Dandouras, I., Yamauchi, M., and the ESCAPE proposal team: European SpaceCraft for the study of Atmospheric Particle Escape (ESCAPE),  
Mission proposals to 2016 ESA's call for M5 Mission, [http://cluster.irap.omp.eu/public/ESCAPE/ESCAPE\\_M5\\_Proposal\\_V1.1.pdf](http://cluster.irap.omp.eu/public/ESCAPE/ESCAPE_M5_Proposal_V1.1.pdf),  
2016.
- Dandouras, I., Yamauchi, M., J. De Keyser, J., Marghitsu, O., Reme, H., Yoshikawa, I., Sakanoi, T., and the ESCAPE proposal team: ESCAPE:  
700 A mission proposal for ESA-M5 to systematically study Exosphere and atmospheric escape using European, Japanese, and US instruments  
(in Japanese), JAXA document SA6000118033, S10-001, <https://repository.exst.jaxa.jp/dspace/handle/a-is/876320>, 2018.
- Darrouzet, F., De Keyser, J., Décréau, P. M. E., El Lemdani-Mazouz, F., and Vallières, X.: Statistical analysis of plasmaspheric plumes with  
Cluster/WHISPER observations, *Ann. Geophys.*, 26, 2403-2417, doi:10.5194/angeo-26-2403-2008, 2008.
- Darrouzet, F., Gallagher, D. L., André, M., Carpenter, D. L., et al., Plasmaspheric density structures and dynamics: Properties observed by  
705 the CLUSTER and IMAGE missions, *Space Sci. Rev.*, 145(1-2), 55-106, doi:10.1007/s11214-008-9438-9, 2009.
- Dungey, J.W.: Interplanetary magnetic field and the auroral zones, *Phys. Rev. Lett.* 6, 47, doi:10.1103/PhysRevLett.6.47, 1961.
- Ebihara, Y., Yamauchi, M., Nilsson, H., Lundin, R., and Ejiri, M.: Wedge-like dispersion of sub-keV ions in the dayside magnetosphere:  
Particle simulation and Viking observation, *J. Geophys. Res.*, 106, 29571-29584, doi:10.1029/2000JA000227, 2001.
- Ebihara, Y., and Ejiri, M.: Numerical Simulation of the Ring Current: Review, *Space Science Reviews*, 105, 377452,  
710 doi:10.1023/A:1023905607888, 2003.
- Ebihara, Y., Ejiri, M., Nilsson, H., Sandahl, I., Grande, M., Fennell, J. F., Roeder, J. L., Weimer, D. R., and Fritz, T. A.: Multiple discrete-  
energy ion features in the inner magnetosphere: 9 February 1998, event, *Ann. Geophys.*, 22, 1297-1304, doi:10.5194/angeo-22-1297-2004,  
2004.
- Ebihara, Y., Kistler, L. M., and Eliasson, L.: Imaging cold ions in the plasma sheet from the Equator-S satellite, *Geophys. Res. Lett.*, 35,  
715 L15103, doi:10.1029/2008GL034357, 2008.
- Ejiri, M.: Trajectory traces of charged particles in the magnetosphere, *J. Geophys. Res.*, 83, 4798-4810, doi:  
<https://doi.org/10.1029/JA083iA10p04798>, 1978.
- Ejiri, M., Hoffman, R. A., and Smith, P. H.: Energetic particle penetration into the inner magnetosphere, *J. Geophys. Res.*, 85, 653-663,  
doi:10.1029/JA085iA02p00653, 1980.
- 720 Eklund, U., Lundin, R., and Sandahl, I: Measurements of O<sup>+</sup> in the high latitude magnetosheath, *Phys. Chem. Earth*, 22, 639-644,  
doi:10.1016/S0079-1946(97)00189-4, 1997.
- Engwall, E., Eriksson, A. I., André, M., Dandouras, I., Paschmann, G., Quinn, J., and Torkar, K.: Low-energy (order 10 eV) ion flow in the  
magnetotail lobes inferred from spacecraft wake observations, *Geophys. Res. Lett.*, 33, L06110, doi:10.1029/2005GL025179, 2006.
- Engwall, E., Eriksson, A. I., Cully, C. M., André, M., Puhl-Quinn, P. A., Vaith, H., and Torbert, R.: Survey of cold ionospheric outflows in  
725 the magnetotail, *Ann. Geophys.*, 27, 3185-3201, doi:10.5194/angeo-27-3185-2009, 2009.



- Eliasson, L., André, M., Eriksson, A., Nordqvist, P., Norberg, O., Lundin, R., Holback, B., Koskinen, H., Borg, H., and Boehm, M. (1994), Freja observations of heating and precipitation of positive ions, *Geophys. Res. Lett.*, 21, 1911-1914, doi:10.1029/94GL01067, 1994.
- Fok, M.-C., Kozyra, J. U., Nagy, A. F., and Cravens, T. E.: Lifetime of ring current particles due to coulomb collisions in the plasmasphere, *J. Geophys. Res.*, 96, 7861-7867, doi:10.1029/90JA02620, 1991.
- 730 Giang, T. T., Hamrin, M., Yamauchi, M., Lundin, R., Nilsson, et al.: Outflowing protons and heavy ions as a source for the sub-keV ring current, *Ann. Geophys.*, 27, 839-849, doi:10.5194/angeo-27-839-2009, 2009.
- Goldstein J.: Plasmasphere response: Tutorial and review of recent imaging results, *Space Sci. Rev.*, 124, 203, doi:10.1007/s11214-006-9105-y, 2006.
- Gringauz, K.I., Kurt, V.G., Moroz, V.I., Shklovskii, I.S.: ionized gas and high energy electrons in the vicinity of the Earth and in the  
735 interplanetary space, *Dokl. Akad. Nauk SSSR*, 132, 1062-1065, 1960.
- Grünwaldt, H., Neugebauer, M., Hilchenbach, M., Bochsler, P., et al.: Venus tail ray observation near Earth, *Geophys. Res. Lett.*, 24, 1163-1166, doi:10.1029/97GL01159, 1997.
- Hamilton, D. C., Gloeckler, G., Ipavich, F. M., Studemann, W., Wilken, B., and Kremser, G.: Ring current development during the great geo- magnetic storm of February 1986, *J. Geophys. Res.*, 93, 14343-14355, doi:10.1029/JA093iA12p14343, 1988.
- 740 Hardy, D. A., Gussenhoven, M. S., and Brautigam, D.: A statistical model of auroral ion precipitation, *J. Geophys. Res.*, 94(A1), 370-392, doi:10.1029/JA094iA01p00370, 1989.
- Harrison J., Kaiser, A., and Vanden, J. M.: Atmospheric oxygen level and the evolution of insect body size, *Proc. R. Soc. B*, 277, 19371946, doi:10.1098/rspb.2010.0001, 2010.
- Hill S. (1976), Influence of atmospheric oxygen concentration on acetylene reduction and efficiency of nitrogen fixation in intact *Klebsiella*  
745 *pneumoniae*, *Microbiol.*, 93, 335-345, doi: 10.1099/00221287-93-2-335.
- Hirahara, M., T. Mukai, E. Sagawa, N. Kaya, and H. Hayakawa, Multiple energy-dispersed ion precipitations in low-latitude auroral oval: Evidence of  $E \times B$  drift effect and up ward flowing ion contribution, *J. Geophys. Res.*, 102, 2513-2530, doi:10.1029/96JA03148, 1997.
- Horwitz, J. L. and Chappell, C. R.: Observations of warm plasma in the dayside plasma trough at geosynchronous orbit, *J. Geophys. Res.*, 84, 7075-7090, doi:10.1029/JA084iA12p07075, 1979.
- 750 Hultqvist, B., Aparicio, B., Borg, H., Arnoldy, R., and Moore, T. E.: Decrease of keV electron and ion fluxes in the dayside magnetosphere during the early phase of magnetospheric disturbances, *Planet. Space Sci.*, 29, 107-126, doi:10.1016/0032-0633(81)90143-4, 1981.
- Hultqvist, B.: Downward ion acceleration at auroral latitudes: cause of parallel electric field, *Ann. Geophys.*, 20, 1117-1136, doi:10.5194/angeo-20-1117-2002, 2002.
- Jordanova, V. K., Farrugia, C. J., Quinn, J. M., Torbert, R. B., Borovsky, J. E., Sheldon, R. B., and Peterson, W. K.: Simulation of  
755 off-equatorial ring current ion spectra measured by Polar for a moderate storm at solar minimum, *J. Geophys. Res.*, 104, 429-436, doi:10.1029/98JA02658, 1999.
- Kistler, L. M., Moukikis, C., Möbius, E., Klecker, B., Sauvaud, J. A., et al.: Contribution of nonadiabatic ions to the cross-tail current in an  $O^+$  dominated thin current sheet, *J. Geophys. Res.*, 110, A06213, doi:10.1029/2004JA010653, 2005.
- Krauss, S., Fichtinger, B., Lammer, H., Hausleitner, W., Kulikov, Yu. N., Ribas, I., Shematovich, V. I., Bisikalo, D., Lichtenegger, H. I.  
760 M., Zaqarashvili, T. V., Khodachenko, M. L., and Hansmeier, A.: Solar flares as proxy for the young Sun: satellite observed thermosphere response to an X17.2 flare of Earth's upper atmosphere, *Ann. Geophys.*, 30, 1129-1141, doi:10.5194/angeo-30-1129-2012, 2012.
- Kronberg, E.A., Ashour-Abdalla, M., Dandouras, I., Delcourt, D. C., et al.: Circulation of heavy ions and their dynamical effects in the magnetosphere: recent observations and models, *Space Sci. Rev.*, 184, 173-235, doi:10.1007/s11214-014-0104-0, 2014.



- Lakhina, G.S. and Tsurutani, B.T. (2017), Satellite drag effects due to uplifted oxygen neutrals during super magnetic storms, *Nonlin. Processes Geophys.*, 24, 745-750, doi:10.5194/npg-24-745-2017, 2017
- 765 Lennartsson, O. W.: ISEE ion composition data with implications for solar wind entry into Earth's magnetotail, *Space Sci. Rev.*, 80, 305-323, doi:10.1023/A:1004982122553, 1997.
- Lennartsson, O. W.: Ion composition aspects of magnetotail plasma flows, *J. Geophys. Res.*, 106, 15621-15634, doi:10.1029/2000JA000427, 2001.
- 770 Lennartsson, O. W., Collin, H. L., and Peterson, W. K.: Solar wind control of Earth's H<sup>+</sup> and O<sup>+</sup> outflow rates in the 15 eV to 33 keV energy range, *J. Geophys. Res.*, 109, A12212, doi:10.1029/2004JA010690, 2004.
- Loesche W.J. (1969), Oxygen sensitivity of various anaerobic bacteria, *Appl. Microbiol.*, 18, 723-727.
- Lundin, R.: Plasma composition and flow characteristics in the magnetospheric boundary layers connected to the polar cusp, in *The Polar Cusp*, edited by J. A. Holtet and A. Egeland, 9, D. Reidel Publishing Comp., 1985.
- 775 Lundin, R., Yamauchi, M., Woch, J., and Marklund G.: Boundary layer polarization and voltage in the 14 MLT region, *J. Geophys. Res.*, 100, 7587-7597, doi:10.1029/94JA02523, 1995.
- Maezawa, K. and Hori, T.: The Distant Magnetotail: Its Structure, IMF Dependence and Thermal Properties, in *New Perspectives on the Earth's Magnetotail*, eds by A. Nishida, D. N. Baker and S. W. H. Cowley, 1-19, AGU, Washington D.C., 1998.
- Maggiolo, R., and Kistler, L.M.: Spatial variation in the plasma sheet composition: Dependence on geomagnetic and solar activity, *J. Geophys. Res.*, 119, 2836-2857, doi:10.1002/2013JA019517, 2014.
- 780 Marcucci, M. F., Bavassano-Cattaneo M. B. Pallochia, G., Amata, E., et al.: Energetic magnetospheric oxygen in the magnetosheath and its response to IMF orientation: Cluster observations, *J. Geophys. Res.*, 109, A07203, doi:10.1029/2003JA010312, 2004.
- Meier R.R., Picone J.M., Drob D., et al.: Remote Sensing of Earth's Limb by TIMED/GUVI: Retrieval of thermospheric composition and temperature, *Earth Space Sci.*, 2, 1-37, doi:10.1002/2014EA000035, 2015.
- 785 Moore T.E., Lundin R., Alcayde D., Andre M., Ganguli S. B., Temerin M. and Yau A.: Source processes in the high-latitude ionosphere, Chapter 2 in *Magnetospheric Plasma Sources and Losses*, edited by B. Hultqvist et al., Kluwer academic publication, *Space Sci. Rev.*, 88, 7-84, doi:10.1023/A:1005299616446, 1999.
- Möbius, E., Tang, L., Kistler L. M., Popecki M., et al.: Species dependent energies in upward directed ion beams over auroral arcs as observed with FAST TEAMS, *Geophys. Res. Lett.*, 25, 2029-032, doi:10.1029/98GL00381, 1998.
- 790 Newell, P. T. and Meng, C. I.: Substorm introduction of 1 keV magnetospheric ions into the inner plasmasphere, *J. Geophys. Res.*, 91, 11133-11145, doi:10.1029/JA091iA10p11133, 1986.
- Newell, P. T., Sotirelis, T., and S. Wing, S.: Seasonal variations in diffuse, monoenergetic, and broadband aurora, *J. Geophys. Res.*, 115, A03216, doi:10.1029/2009JA014805, 2010.
- Nilsson, H., Waara, M., Arvelius, S., Marghitu, O., et al.: Characteristics of high altitude oxygen ion energization and outflow as observed by Cluster: a statistical study, *Ann. Geophys.*, 24(3), 1099-1112, doi:10.5194/angeo-24-1099-2006, 2006.
- 795 Nilsson, H., Barghouthi, I. A., Slapak, R., Eriksson, A., and André, M.: Hot and cold ion outflow: spatial distribution of ion heating, *J. Geophys. Res.*, 117, A11 201, doi:10.1029/2012JA017974, 2012.
- Nilsson, H., Hamrin, M., Pitkänen, T., Karlsson, T., Slapak, R., Andersson, L., Gunell, H., Schillings, A., and Vaivads A.: Oxygen ion response to proton bursty bulk flows, *J. Geophys. Res., Space Physics*, 121, 7535-7546, doi:10.1002/2016JA022498, 2016.
- 800 Norqvist, P., André, M., Eliasson, L., Eriksson, A.I., Blomberg, L., H. Lühr, and Clemmons, J.H.: Ion cyclotron heating in the dayside magnetosphere, *J. Geophys. Res.*, 101(A6), 13179-13193, doi:10.1029/95JA03596, 1996.



- Norqvist, P., Andre, M., and Tyrland, M.: A statistical study of ion energization mechanisms in the auroral region, *J. Geophys. Res.*, 103, 23459-23474, doi:10.1029/98JA02076, 1998.
- Nosé, M., Ieda, A., and Christon, S. P., Geotail observations of plasma sheet ion composition over 16 years: On variations of average plasma  
805 ion mass and O<sup>+</sup> triggering substorm model, *J. Geophys. Res.*, 114, A07223, doi:10.1029/2009JA014203, 2009.
- Ohtani, S., Potemra, T. A., Newell, P. T., Zanetti, L. J., Iijima, T., Watanabe, M., Yamauchi, M., Elphinstone, R. D., de la Beaujardiere, O.,  
and Blomberg, L.G.; Simultaneous prenoon and postnoon observations of three field-aligned current systems from Viking and DMSP-F7,  
*J. Geophys. Res.*, 100, 119-136, doi:10.1029/94JA02073, 1995.
- Ohtani, S., Shay, M. A., and Mukai, T.: Temporal structure of the fast convective flow in the plasma sheet: Comparison between observations  
810 and two-fluid simulations, *J. Geophys. Res.*, 109, A03210, doi:10.1029/2003JA010002, 2004.
- Olsen, R. C., Shawhan, S. D., Gallagher, D. L., Green, J. L., Chappell, C. R., and Anderson, R. R.: Plasma observations at the Earth's  
magnetic equator, *J. Geophys. Res.*, 92, 2385-2407, doi:10.1029/JA092iA03p02385, 1987.
- Olsen, R. C.: The density minimum at the Earth's magnetic equator, *J. Geophys. Res.*, 97, 1135-1150, doi:10.1029/91JA02719, 1992.
- Øieroset, M., M. Yamauchi, L. Liszka and S. P. Christon (2000), Energetic ion outflow from the dayside ionosphere and its relationship to  
815 the interplanetary magnetic field and substorm activity". *J. Atmos. Terres. Phys.*, 485-493, doi:10.1016/S1364-6826(00)00016-X, 2000.
- Park, C. G. (1974), Some features of plasma distribution in plasmasphere deduced from antarctic whistlers, *J. Geophys. Res.*, 79(1), 169-173.
- Peterson, W. K., Collin, H. L., Yau, A. W., and Lennartsson, O. W.: Polar/TIMAS observations of suprathermal ion outflow during solar  
minimum conditions, *J. Geophys. Res.*, 106, 6059, doi:10.1029/2000JA003006, 2001.
- Peterson, W. K., Collin, H. L., Lennartsson, O. W., and Yau, A. W.: Quiet time solar illumination effects on the fluxes and characteristic  
820 energies of ionospheric outflow, *J. Geophys. Res.*, 111, A11S05, doi:10.1029/2005JA011596, 2006.
- Peterson, W. K., Andersson, L., Callahan, B. C., Collin, H. L., Scudder, J. D., and Yau, A. W.: Solar-minimum quiet time ion energization  
and outflow in dynamic boundary related coordinates, *J. Geophys. Res.*, 113, A07222, doi:10.1029/2008JA013059, 2008.
- Potemra, T. A.: Sources of large-scale Birkeland currents, in *Physical signatures of magnetospheric boundary layer process*, edited by J. A.  
Holtet, and A. Egeland, pp. 3-27, Kluwer Academic Publishers, Dordrecht, Netherlands, 1994.
- 825 Pollock, C. J., Chandler, M. O., Moore, T. E., Waite, J. H., Chappell, C. R., and Gurnett, D. A.: A survey of upwelling ion event characteristics,  
*J. Geophys. Res.*, 95, 18969-18980, doi:10.1029/JA095iA11p18969, 1990.
- Quinn, J. M. and McIlwain, C. E.: Bouncing ion clusters in the Earth's magnetosphere, *J. Geophys. Res.*, 84, 7365-7370,  
doi:10.1029/JA084iA12p07365, 1979.
- Rème, H., Aoustin, C., Bosqued, J. M., Dandouras, I., et al.: First multispacecraft ion measurements in and near the Earth's magnetosphere  
830 with the identical Cluster ion spectrometry (CIS) experiment, *Ann. Geophys.*, 19, 1303-1354, doi:10.5194/angeo-19-1303-2001, 2001.
- Ribas, S., Guinan, E. F., Güdel, M., and Audard, M.: Evolution of the solar activity over time and effects on planetary atmospheres. I.  
High-energy irradiances (1-1700 Å), *Astrophys. J.*, 622, 680-694, doi:10.1086/427977, 2005.
- Sandel, B. R., and Denton, M. H.: Global view of refilling of the plasmasphere, *Geophys. Res. Lett.*, 34, L17102,  
doi:10.1029/2007GL030669, 2007.
- 835 Sandel, B. R.: Composition of the plasmasphere and implications for refilling, *Geophys. Res. Lett.*, 38, L14104, doi:10.1029/2011GL048022,  
2011.
- Sandhu, J. K., Yeoman, T. K., Fear, R. C., and Dandouras, I.: A statistical study of magnetospheric ion composition along the geomagnetic  
field using the Cluster spacecraft for L values between 5.9 and 9.5, *J. Geophys. Res.*, 121, 2194-2208, doi:10.1002/2015JA022261, 2016.



- Sauvaud, J.-A., Crasnier, J., Mouala, K., Kovrazhkin, R. A. and Jorjio, N. V.: Morning sector ion precipitation following substorm injections, *J. Geophys. Res.*, 86, 3430-3438, doi:10.1029/JA086iA05p03430, 1981.
- 840 J.-A. Sauvaud, Louarn, P., Fruit, G., Stenuit, H., et al.: Case studies of the dynamics of ionospheric ions in the Earth's magnetotail, *J. Geophys. Res.*, 109, A01212, doi:10.1029/2003JA009996, 2004.
- Schillings, A., Nilsson, H., Slapak, R., Yamauchi, M., and Westerberg, L.-G.: Relative outflow enhancements during major geomagnetic storms - Cluster observations, *Ann. Geophys.*, 35, 1341-1352, doi:10.5194/angeo-35-1341-2017, 2017.
- 845 Schillings, A., Slapak, R., Nilsson, N., Yamauchi, M., Dandouras, I., and Westerberg, L.-G.: Earth atmospheric loss through the plasma mantle and its dependence on solar wind parameters, *Earth Planet Space*, 71, 70, doi:10.1186/s40623-019-1048-0, 2019.
- Seki, K., Elphic, R. C., Hirahara, M., Terasawa, T., and Mukai, T.: On atmospheric loss of oxygen ions from Earth through magnetospheric processes, *Science*, 291, 1939-1941, doi:10.1126/science.1058913, 2001.
- Seki, K., Hirahara, M., Hoshino, M., Terasawa, T., Elphic, R. C., Saitok, Y., Mukaik, T., Hayakawa, H., Kojima, H., and Matsumoto, H.:  
850 Cold ions in the hot plasma sheet of Earth's magnetotail, *Nature*, 422, 589-592, doi:10.1038/nature01502, 2003.
- Sergeev, V.A., Malkov, M., Mursula, K.: Testing the isotropic boundary algorithm method to evaluate the magnetic field configuration in the tail, *J. Geophys. Res.* 98, 7609-7620, doi:10.1029/92JA02587, 1993.
- Shelley, E. G., Johnson, R. G., and Sharp, R. D.: Satellite observations of energetic heavy ions during a geomagnetic storm, *J. Geophys. Res.*, 77, 6104-6110, doi:10.1029/JA077i031p06104, 1972.
- 855 Sibeck, D. G., McEntire, R. W., Lui, A. T. Y., Lopez, R. E., Krimigis, S. M., Decker, R. B., Zanetti, L. J., and Potemra, T. A. (1987), Energetic magnetospheric ions at the dayside magnetopause: Leakage or merging?, *J. Geophys. Res.*, 92, 12097-12114, doi:10.1029/JA092iA11p12097
- Sibeck, D. G., Paschmann, G., Treumann, R. A., et al.: Plasma transfer processes at the magnetopause, Chapter 5 in *Magnetospheric Plasma Sources and Losses*, edited by B.Hultqvist et al., Kluwer academic publication, *Space Sci. Rev.*, 88, 207-283,  
860 doi:10.1023/A:1005255801425, 1999.
- Slapak, R., Nilsson, H., and Westerberg, L. G.: A statistical study on O<sup>+</sup> flux in the dayside magnetosheath, *Ann. Geophys.*, 31, 1005-1010, doi:10.5194/angeo-31-1005-2013, 2013.
- Slapak, R., Schillings, A., Nilsson, H., Yamauchi, M., Westerberg, L.G., and Dandouras, I.: Atmospheric loss from the dayside open polar region and its dependence on geomagnetic activity: Implications for atmospheric escape on evolutionary time scales, *Ann. Geophys.*, 35,  
865 721-731, doi:10.5194/angeo-35-721-2017, 2017a.
- Slapak R., Hamrin M., Pitkänen T., Yamauchi M., Nilsson H., Karlsson T., and Schillings A.: Quantification of the total ion transport in the near-Earth plasma sheet, *Ann. Geophys.*, 35, 869-877, doi:10.5194/angeo-35-869-2017, 2017b.
- Su, Y. J., Horwitz, J. L., Moore, T. E., Giles, B. L., Chandler, M. O., Craven, P. D., Hirahara, M., and Pollock, C. J.: Polar wind survey with the Thermal Ion Dynamics Experiment/Plasma Source Instrument suite aboard POLAR, *J. Geophys. Res.*, 103, 29305-29337,  
870 doi:10.1029/98JA02662, 1998.
- Tian, F., Kasting, J. F., Liu, H.-L., and Roble, R. G.: Hydrodynamic planetary thermosphere model: 1. Response of the Earth's thermosphere to extreme solar EUV conditions and the significance of adiabatic cooling, *J. Geophys. Res.*, 113, E05008, doi:10.1029/2007JE002946, 2008.
- Vasyliunas, V.M. (1995), Multiple-branch model of the open magnetopause, *Geophys. Res. Lett.*, 22, 1145-1147, doi:10.1029/95GL01068.



- 875 Vallat, C., Ganushkina, N., Dandouras, I., Escoubet, C. P., Taylor, M. G. G. T., Laakso, H., Masson, A., Sauvaud, J.-A., Rème, H., and Daly, P.: Ion multi-nose structures observed by Cluster in the inner Magnetosphere, *Ann. Geophys.*, 25, 171-190, doi:10.5194/angeo-25-171-2007, 2007.
- Waara, M., Slapak, R., Nilsson, H., Stenberg, G., André, M., and Barghouthi, I. A.: Statistical evidence for O<sup>+</sup> energization and outflow caused by wave-particle interaction in the high altitude cusp and mantle, *Ann. Geophys.*, 29, 945-954, doi:10.5194/angeo-29-945-2011, 880 2011.
- Walker, R., Terasawa, T., Christon, S.P., Angelopoulos, V., et al.: Source and loss processes in the magnetotail, *Space Sci. Rev.*, 88, 285-353, doi:10.1023/A:1005207918263, 1999.
- Waite, J. H., Gallagher, D. L., Chandler, M. O., Olsen, R. C., et al.: Plasma and field observations of a Pc 5 wave event, *J. Geophys. Res.*, 91, 11147-11161, doi:10.1029/JA091iA10p11147, 1986.
- 885 Welling, D. T., Jordanova, V. K., Zaharia, S. G., Glocer, A., and Toth, G.: The effects of dynamic ionospheric outflow on the ring current, *J. Geophys. Res.*, 116, A00J19, doi:10.1029/2010JA015642, 2011.
- Welling, D.T., André, M., Dandouras, I., Delcourt, D., et al.: The Earth: plasma sources, losses, and transport processes, *Space. Sci. Rev.*, 192, 145, doi:10.1007/s11214-015-0187-2, 2015.
- Winglee, R. M., Chua, D., Brittnacher, M., Parks, G. K., and Lu, G. (2002), Global impact of ionospheric outflows on the dynamics of the 890 magnetosphere and cross-polar cap potential, *J. Geophys. Res.*, 107(A9), 1237, doi:10.1029/2001JA000214.
- Winningham, D. J., F. Yasuhara, S.-I. Akasofu, and W. J. Heikkila (1975), The latitudinal morphology of 10 eV to 10 keV electron fluxes during quiet and disturbed times in the 2100-0300 MLT sector, *J. Geophys. Res.*, 80, 3148.
- Woch, J., and Lundin, R. (1993), The low-latitude boundary layer at mid-altitudes: Identification based on Viking hot plasma data, *Geophys. Res. Lett.*, 20, 979-982.
- 895 Wood, B. E.: The solar wind and the Sun in the past, *Space Sci. Rev.*, 126, 3-14, doi:10.1007/s11214-006-9006-0, 2006.
- Yamauchi, M., and Araki, T.: The interplanetary magnetic field By-dependent field-aligned current in the dayside polar cap under quiet conditions, *J. Geophys. Res.*, 94, 2684-2690, doi:10.1029/JA094iA03p02684, 1989.
- Yamauchi, M., Lundin, R., and Woch, J.: The interplanetary magnetic field By effects on large-scale field-aligned currents near local noon: Contributions from cusp part and noncusp part, *J. Geophys. Res.*, 98, 5761-5767, doi:10.1029/92JA02934, 1993a.
- 900 Yamauchi, M., Lundin, R., Eliasson, L., and Norberg, O.: Meso-scale structures of radiation belt/ring current detected by low-energy ions, *Adv. Space Res.*, 17, 171-174, doi:10.1016/0273-1177(95)00531-I, 1996a.
- Yamauchi, M., R. Lundin, K. Mursula, G. Marklund, and T. A. Potemra.: Dayside Pc5 pulsation detected by Viking ion data at L=4, *Geophys. Res. Lett.*, 23, 2517-2520, doi:10.1029/96GL02140, 1996b.
- Yamauchi, M., Nilsson, H., Eliasson, L., Norberg, O., Boehm, M. et al.: Dynamic response of the cusp morphology to the solar wind: A case 905 study during passage of the solar wind plasma cloud on February 21, 1994, *J. Geophys. Res.*, 101, 24675-24687, doi:10.1029/96JA01873, 1996c.
- Yamauchi, M., and Lundin R.: The wave-assisted cusp model: Comparison to low-altitude observations, *Phys. Chem. Earth*, 22, 729-734, doi:10.1016/S0079-1946(97)00203-6, 1997.
- Yamauchi, M., R. Lundin, L. Eliasson, D. Winningham, H. Reme, C. Vallat, I. Dandouras, and Cluster-CIS team.: Structures of sub-keV 910 ions inside the ring current region, in "The Inner Magnetosphere: Physics and Modeling", AGU Geophys. Monograph, 155, edited by T.I. Pulkkinen, N.A. Tsyganenko, and R. Friedel, 41-46, doi:10.1029/155GM05, 2005a.



- Yamauchi, M., Eliasson, L., Lundin, R., and Norberg, O.: Unusual heavy ion injection events observed by Freja, *Ann. Geophys.*, 23, 535-543, doi:10.5194/angeo-23-535-2005, 2005b
- 915 Yamauchi, M. and Lundin, R.: Sub-keV ring current ions as the tracer of substorm injection, *Ann. Geophys.*, 24, 355–366, 10.5194/angeo-24-355-2006, 2006.
- Yamauchi, M., Brandt, P. C., Ebihara, Y., Dandouras, I., Nilsson, H., Lundin, R., Rème, H., Vallat, C., Lindqvist, P.-A., Balogh, A., and Daly, P. W.: Source location of the wedge-like dispersed ring current in the morning sector during a substorm, *J. Geophys. Res.*, 111, A11S09, 10.1029/2006JA011621, 2006a.
- 920 Yamauchi, M., Iyemori, Y., Frey, H. and Henderson, M.: Unusually quick development of a 4000 nT substorm during the initial 10 min of the 29 October 2003 magnetic storm, *J. Geophys. Res.*, 111, A04217, doi:10.1029/2005JA011285, 2006b.
- Yamauchi, M. and Wahlund, J.-E.: Role of the ionosphere for the atmospheric evolution of planets, *Astrobiology J.*, 7, 783-800, doi:10.1089/ast.2007.0140, 2007.
- Yamauchi, M., Ebihara, Y., Dandouras, I., and Rème, H.: Dual source populations of substorm-associated ring current ions, *Ann. Geophys.*, 27, 1431-1438, doi:10.5194/angeo-27-1431-2009, 2009a
- 925 Yamauchi, M., Dandouras, I., Daly, P. W., Stenberg, G., Frey, H. U., et al.: Magnetospheric solitary structure maintained by 3000 km/s ions as a cause of westward moving auroral bulge at 19 MLT, *Ann. Geophys.*, 27, 2947-2969, doi:10.5194/angeo-27-2947-2009, 2009b.
- Yamauchi, M., Dandouras, I., Rème, H., and El-Lemdani Mazouz, F.: Equatorially confined warm trapped ions at around 100 eV near the plasmopause, *Geophys. Res. Lett.*, 39, L15101, doi:10.1029/2012GL052366, 2012.
- 930 Yamauchi, M., Dandouras, I., Rème, H., Lundin, R., and Kistler, L. M.: Cluster observation of few-hour-scale evolution of structured plasma in the inner magnetosphere, *Ann. Geophys.*, 31, 1569-1578, doi:10.5194/angeo-31-1569-2013, 2013.
- Yamauchi, M., Dandouras, I., Rème, H., and Nilsson, H.: Cluster observations of hot He<sup>+</sup> events in the inner magnetosphere, *J. Geophys. Res.*, 119, 2706-2716, doi:10.1002/2013JA019724, 2014a.
- Yamauchi, M., Ebihara, Y., Nilsson, H., and Dandouras, I.: Ion drift simulation of sudden appearance of sub-keV structured ions in the inner magnetosphere, *Ann. Geophys.*, 32, 83-90, doi:10.5194/angeo-32-83-2014, 2014b.
- 935 Yamauchi, M., Hara, T., Lundin, R., Dubinin, E., Fedorov, A., Sauvaud, J.-A., Frahm, R.A., Ramstad, R., Futaana, Y., Holmström, M., and Barabash, S.: Seasonal variation of Martian pick-up ions: evidence of breathing exosphere, *Planet. Space Sci.*, 119, 54-61, 2015. doi:10.1016/j.pss.2015.09.013, 2015.
- Yamauchi, M. and Slapak R.: Cusp current system: an energy source view, in "Electric Currents in Geospace and Beyond", *AGU Geophys. Monogr.*, 235, eds A. Keiling, O. Marghita, and M. Wheatland, Chapter 20, 339-358, 2018. doi: 10.1002/9781119324522.ch20, 2018a.
- 940 Yamauchi, M. and Slapak R.: Energy conversion through mass loading of escaping ionospheric ions for different Kp values, *Ann. Geophys.*, 36, 1-12, doi:10.5194/angeo-36-1-2018, 2018b.
- Yamauchi, M., Sergienko T., Enell C.-F., Schillings A., Slapak R., Johnsen M. G., Tjulin A., and Nilsson H.: Ionospheric response observed by EISCAT during the September 6-8, 2017, space weather event: overview, *Space Weather*, 16, 1437-1450, doi:10.1029/2018SW001937, 2018.
- 945 Yau, A. W., and Whalen, B. A.: Auroral ion composition during large magnetic storms, *Can. J. Physics*, 70, 500-509, doi:10.1139/p92-085, 1992.
- Zoennchen, J. H., Nass, U., and Fahr, H. J.: Terrestrial exospheric hydrogen density distributions under solar minimum and solar maximum conditions observed by the TWINS stereo mission, *Ann. Geophys.*, 33, 413-426, doi:10.5194/angeo-33-413-2015, 2015.



Zoennchen J. H., Nass U, Fahr H.J., and Goldstein J.: The response of the H geocorona between 3 and 8 Re to geomagnetic disturbances  
950 studied using TWINS stereo Lyman- $\alpha$  data, *Ann. Geophys.*, 35, 171-179, doi:10.5194/angeo-35-171-2017, 2017.